Draping Woven Sheets

P. D. Howell H. Ockendon J. R. Ockendon

OCIAM
Mathematical Institute
Andrew Wiles Building
Oxford OX2 6GG
UK

September 30, 2020

Abstract

Motivated by the manufacture of carbon-fibre components, this paper considers the smooth draping of loosely woven fabric over rigid obstacles, both smooth and non-smooth. The draped fabric is modelled as the continuum limit of a Chebyshev net of two families of short rigid rods that are freely pivoted at their joints. This approach results in a system of nonlinear hyperbolic partial differential equations whose characteristics are the fibres in the fabric. The analysis of this system gives useful information about the drapability of obstacles of many shapes and also poses interesting theoretical questions concerning well-posedness, smoothness and computability of the solutions.

1 Introduction

This paper is motivated by the possibility of manufacturing carbon fibre structures by draping woven carbon fibre sheets over rigid obstacles of a desired shape; after draping, resin is applied and baked as described in [2]. Carbon fibre sheets are composed of two families of inextensible fibres woven fairly loosely so that they can undergo shear, by which we mean a variation in the angle between the fibres of each family. Originally the families are orthogonal, and we assume that they can rotate freely relative to each other but that there is no sliding at the contact points between the fibres. By draping we mean that the sheet is brought into contact smoothly with a rigid obstacle of the desired shape, possibly by the application of forces that induce suitably chosen shears. The shearing of the material allows us to drape non-developable surfaces smoothly in contrast to "origami-draping", which is only possible for developable surfaces.

Many models for fibre sheet deformation have been considered in the literature, ranging from

1. discrete models for systems of reticulated woven elastic rods [1, 17];
2. networks of inextensible rods, the simplest being the "Chebyshev nets" of equal inextensible rods that can shear but are pinned at the joints [9, 13];
3. homogenised elastic and/or plastic models [4, 8, 14, 15, 23, 24].

In this paper we will consider the even simpler model of the continuum limit of a Chebyshev network as the rod length tends to zero, so that a sheet is composed of two families of fibres that deform isometrically onto a given obstacle. The obstacle represents a surface in which the the fibres are required to lie, defined for example by an equation of the form $f(\boldsymbol{r}) = 0$, where $\boldsymbol{r} = (x, y, z)^{\mathrm{T}} \in \mathbb{R}^3$. Our task is then to find a suitable parametrisation $\boldsymbol{r} = \boldsymbol{r}(u, v)$ of the surface, where the two families of fibres are given by u = constant and v = constant and u, v are distances measured along the fibres. Since the infinitesimal length between successive joints is supposed to be conserved, the parametrisation must satisfy the constraints

$$|\boldsymbol{r}_u|^2 = |\boldsymbol{r}_v|^2 = 1, \tag{1}$$

along with $f\big(\boldsymbol{r}(u, v)\big) = 0$.

Most of this paper will be devoted to considering solutions of (1) subject to physically relevant boundary conditions. Once we have solved for $\boldsymbol{r}(u, v)$, the "shear angle" between the two families of fibres is found from

$$\cos\gamma = \boldsymbol{r}_u \cdot \boldsymbol{r}_v. \tag{2}$$

The angle γ is important not only analytically and geometrically, but also because the model breaks down as $\gamma \to 0$. In practice, γ is initially equal to $\pi/2$ in the undeformed fabric, and creasing will occur if γ decreases below a finite value which depends on the width and spacing of the fibres.

Before we start, we recall some features of this well-studied model.

(i) As shown in [25], the Gaussian curvature $K(u, v)$ satisfies

$$K = \frac{(\boldsymbol{r}_{uu} \cdot \boldsymbol{n})(\boldsymbol{r}_{vv} \cdot \boldsymbol{n}) - (\boldsymbol{r}_{uv} \cdot \boldsymbol{n})^2}{(\boldsymbol{r}_u)^2(\boldsymbol{r}_v)^2 - (\boldsymbol{r}_u \cdot \boldsymbol{r}_v)^2}, \tag{3}$$

where $\boldsymbol{n}$ is the unit normal to the obstacle, and hence it follows that the shear angle satisfies

$$\frac{\partial^2\gamma}{\partial u \partial v} + K\sin\gamma = 0. \tag{4}$$

We note that when the obstacle is a sphere of radius R, then $K = 1/R^2$ and (4) becomes the Sine–Gordon equation, which was derived by [7] and has been applied to fabric drape in [9, 16].

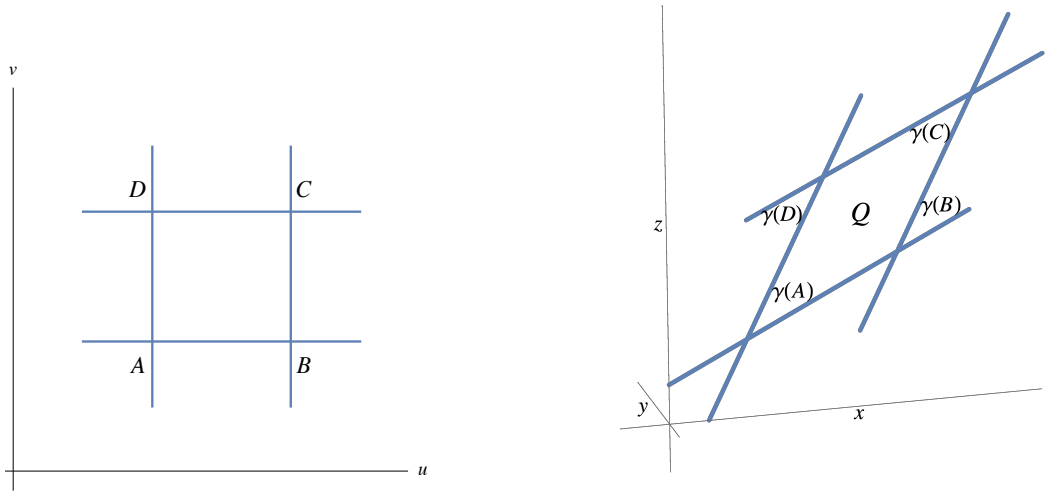

(a) (b)

Figure 1: (a) A rectangle in the (u, v)-plane. (b) The corresponding quadrilateral Q in $\mathbb{R}^3$.

(ii) If $K = 0$, so that the obstacle is a developable surface, then (4) shows that draping can occur with $\gamma =$ constant. On the other hand, (4) also shows that the shear angle must vary when we attempt to drape any surface that is not developable.

(iii) By integrating (4) over the interior Q of a quadrilateral in the sheet bounded by fibres $u =$ constant and $v =$ constant, one obtains a version of the Gauss–Bonnet Theorem [7, 26], namely

$$\iint_Q K \, \mathrm{d}S = \gamma(B) - \gamma(A) + \gamma(D) - \gamma(C), \tag{5}$$

where A, B, C and D are the vertices of Q, as illustrated in Figure 1. The result (5) puts a limit on how much of a non-developable surface may be draped without creasing, since the condition $0 < \gamma < \pi$ may be satisfied only if

$$-2\pi < \iint_Q K \, \mathrm{d}S < 2\pi. \tag{6}$$

For an obstacle that is finite and simply-connected, with Euler characteristic equal to 2, the constraint (6) shows that it is impossible to drape the entire obstacle before the shear angle reaches zero or π.

(iv) It is frequently convenient to parametrise the obstacle, say in the form $\boldsymbol{r} = \boldsymbol{r}(\xi, \eta)$, so that (1) reduces to a system of nonlinear partial differential equations for $\xi(u, v)$ and $\eta(u, v)$, namely

$$E\xi_u^2 + 2F\xi_u\eta_u + G\eta_u^2 = E\xi_v^2 + 2F\xi_v\eta_v + G\eta_v^2 = 1, \tag{7}$$

where $\{E, F, G\}$ are the components of the first fundamental form. For example, if we use Cartesian coordinates (x, y) with $\boldsymbol{r}(x, y) = \big(x, y, z(x, y)\big)^{\mathrm{T}}$, then we can set $(\xi, \eta) = (x, y)$ in (7), with

$$E = 1 + z_x^2, \qquad F = z_x z_y, \qquad G = 1 + z_y^2. \tag{8}$$

(v) For an axisymmetric obstacle given in terms of cylindrical polar coordinates (r, θ) by $\boldsymbol{r}(r, \theta) = \big(r\cos\theta, r\sin\theta, Z(r)\big)^{\mathrm{T}}$, (7) becomes

$$\big(1 + Z'(r)^2\big)\, r_u^2 + r^2\theta_u^2 = \big(1 + Z'(r)^2\big)\, r_v^2 + r^2\theta_v^2 = 1. \tag{9}$$

Similarity solutions of (9) are possible which lead to a formulae for $r(u, v)$ and $\theta(u, v)$ in terms of Jacobi elliptic functions, and we will see examples of this approach in §3. The importance of such solutions in the engineering and visualisation communities has been discussed in [9, 16].

(vi) By cross-differentiation, the problem (7) may be reduced to a quasilinear system, as shown for example by Servant [21, 22] and Bianchi [3]. Several existence proofs for Chebyshev nets are based on analysis of Servant's equations; see for example [10, 20].

With these points in mind, we begin in §2 by considering the well-posedness of (1) subject to boundary conditions appropriate for draping and the possible drapings for a plane. Then in §3 we look at local and global draping of smooth obstacles with prescribed positive or negative Gaussian curvature. We show some examples where exact solutions are available, as well as a numerical approach for draping an arbitrary axisymmetric obstacle. These solutions reveal the possibility that γ can tend to zero for finite values of u, v, and we analyse the local fibre geometry near such points. In §4, we go on to consider first local and then global solutions for some non-smooth piece-wise developable obstacles, that have edges across which the normal is discontinuous and which may lead to singularities in the draped configuration [5, 11]. The situation is more complicated when the obstacle has a corner or vertex, and we show that conical obstacles can only be draped if γ is allowed to have appropriate jumps along certain generators. We summarise our work in §5.

2 Well-posedness of the model

We proceed to classify the problem (1), which we expect to be hyperbolic in view of (4). We first follow a procedure analogous to Charpit's method [12]. Thus we consider the Cauchy problem for the system (7) in which $(\xi, \eta) = \big(X(t), Y(t)\big)$ are prescribed on a curve Γ in the (u, v)-plane parametrised by $(u, v) = \big(U(t), V(t)\big)$. On this curve the functions

$$(p, q, r, s) = (\xi_u, \eta_u, \xi_v, \eta_v) \tag{10}$$

can be determined in principle by seeking real solutions of the simultaneous equations

$$Ep^2 + 2Fpq + Gq^2 = 1, \qquad Er^2 + 2Frs + Gs^2 = 1, \tag{11a}$$

$$\dot{U}p + \dot{V}r = \dot{X}, \qquad \dot{U}q + \dot{V}s = \dot{Y}. \tag{11b}$$

Note that, in view of the squares in (11a), we will also need extra information about the orientation of the sheet to ensure uniqueness.

We next examine whether it is possible to solve uniquely for the first-order derivatives of (p, q, r, s) on Γ; if so, we expect to be able to solve uniquely for (p, q, r, s) when (u, v) is sufficiently close to Γ. Assuming sufficient smoothness, we differentiate the partial differential equations (11a) with respect to u and v, and the boundary conditions (11b) with respect to t, to obtain

$$(Ep + Fq)p_u + (Fp + Gq)q_u = H_1, \qquad (Ep + Fq)p_v + (Fp + Gq)q_v = H_2, \tag{12a}$$

$$(Er + Fs)r_u + (Fr + Gs)s_u = H_3, \qquad (Er + Fs)r_v + (Fr + Gs)s_v = H_4, \tag{12b}$$

$$\dot{U}^2 p_u + \dot{U}\dot{V}(p_v + r_u) + \dot{V}^2 r_v = H_5, \qquad \dot{U}^2 q_u + \dot{U}\dot{V}(q_v + s_u) + \dot{V}^2 s_v = H_6, \tag{12c}$$

where the right-hand sides H_i only depend on undifferentiated terms which are in principle known on Γ. In addition, compatibility demands that

$$r_u - p_v = 0, \qquad s_u - q_v = 0. \tag{12d}$$

The determinant of the system (12) of eight linear equations for the derivatives of (p, q, r, s) is given by

$$\Delta = \left(EG - F^2\right) \sin^2 \gamma \, \dot{U}^2 \dot{V}^2. \tag{13}$$

The first derivatives are thus uniquely determined on Γ unless $\Delta = 0$. The first factor in (13) is strictly positive, and it follows that the system (7) is hyperbolic in the sense that it has real characteristics $u =$ constant and $v =$ constant, away from points where $\sin \gamma = 0$ and the two families of characteristics become parallel. Thus we expect to have a well-posed problem when we prescribe Cauchy data on a curve which is not a characteristic, or when we prescribe either ξ or η on intersecting characteristics (Goursat data, see [12]). The latter is most relevant to the draping problem when we typically prescribe the position of two intersecting fibres so that, for example, $\xi = 0$ on $v = 0$ and $\eta = 0$ on $u = 0$.

The above analysis may be condensed if the parametrisation $\boldsymbol{r}(\xi, \eta)$ is assumed to be orthogonal; this can always be achieved, at least locally, for example by choosing $\xi =$ constant and $\eta =$ constant to be lines of curvature [26]. Thus the first fundamental form is diagonal, so $F = 0$ in (7), and we can introduce the scaling factors by $h_1(\xi, \eta) = |\boldsymbol{r}_\xi(\xi, \eta)| = E^{1/2}$, and $h_2(\xi, \eta) = |\boldsymbol{r}_\eta(\xi, \eta)| = G^{1/2}$. Equations (7) then reduce to

$$h_1(\xi, \eta)^2 \xi_u^2 + h_2(\xi, \eta)^2 \eta_u^2 = 1, \qquad h_1(\xi, \eta)^2 \xi_v^2 + h_2(\xi, \eta)^2 \eta_v^2 = 1, \tag{14}$$

and the shear angle satisfies

$$\cos \gamma = h_1(\xi, \eta)^2 \xi_u \xi_v + h_2(\xi, \eta)^2 \eta_u \eta_v. \tag{15}$$

We may now define direction angles $\alpha(u, v)$ and $\beta(u, v)$ for the curves $v =$ constant and $u =$ constant, respectively, so that

$$\xi_u = \frac{\cos \alpha}{h_1(\xi, \eta)}, \qquad \eta_u = \frac{\sin \alpha}{h_2(\xi, \eta)}, \qquad \xi_v = \frac{\cos \beta}{h_1(\xi, \eta)}, \qquad \eta_v = \frac{\sin \beta}{h_2(\xi, \eta)}, \tag{16}$$

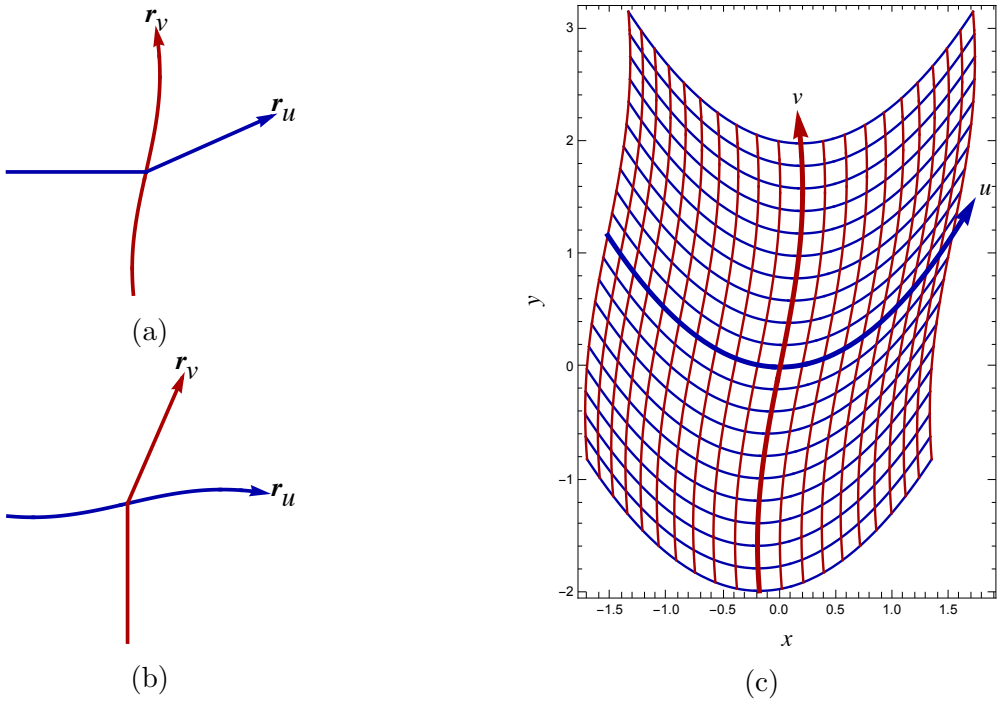

Figure 2: Schematic showing (a) a jump in $\boldsymbol{r}_u$ across a fibre $u =$ constant and (b) a jump in $\boldsymbol{r}_v$ across a fibre $v =$ constant.

and

$$\gamma = \beta - \alpha. \tag{17}$$

Compatibility between the equations (16) requires that α and β satisfy

$$\alpha_v = \frac{h_{1\eta}\cos\beta - h_{2\xi}\sin\beta}{h_1 h_2}, \qquad \beta_u = \frac{h_{1\eta}\cos\alpha - h_{2\xi}\sin\alpha}{h_1 h_2}, \tag{18}$$

which, together with two of (16), form a 4×4 semilinear system for $(\xi, \eta, \alpha, \beta)$ with the fibres being repeated characteristics.

Since the fibres themselves are required to be continuous, we must insist that ξ and η are continuous functions of u and v. However, the semilinear system (18) admits solutions in which α and/or β, and thus γ, have jumps across characteristics. In particular, α may have a jump across a fibre $u =$ constant and β may have jump across a fibre $v =$ constant; the two possibilities are illustrated in Figures 2(a) and 2(b), respectively.

The simplest case occurs if the obstacle is a plane, in which case we can just take $(\xi, \eta) = (x, y)$ and $h_1 = h_2 = 1$ so that $\alpha = \alpha(u)$ and $\beta = \beta(v)$. We may determine a particular solution by specifying two non-parallel initial fibres, leading to a Goursat problem in which boundary data are given on two intersecting characteristics $u =$ constant and $v =$ constant.

For example, suppose we take the fibres $u = 0$ and $v = 0$ to be given by $x = \frac{1}{5}\sin y$ and $y = x^2/2$, respectively, as indicated by the thicker curves in Figure 2(c). This choice

imposes the initial data $\boldsymbol{r}(u,0)=\boldsymbol{f}(u)$ and $\boldsymbol{r}(0,v)=\boldsymbol{g}(v)$ on the characteristics $v=0$ and $u=0$, where

$$\boldsymbol{f}(u)=\begin{pmatrix} f_1(u) \\ f_1(u)^2/2 \end{pmatrix}, \qquad \boldsymbol{g}(v)=\begin{pmatrix} \frac{1}{5}\sin\big(g_2(v)\big) \\ g_2(v) \end{pmatrix}, \tag{19}$$

with f_1 and g_2 chosen to ensure that $|\boldsymbol{f}'|\equiv 1\equiv|\boldsymbol{g}'|$ and $f_1(0)=g_2(0)=0$. The resulting planar mesh, given by

$$\boldsymbol{r}(u,v)=\boldsymbol{f}(u)+\boldsymbol{g}(v), \tag{20}$$

is shown in Figure 2(c).

Although draping on a plane may appear trivial, solutions such as the one shown in Figure 2(c) are useful when considering piecewise developable obstacles, as we will see in §4. First, we study smooth obstacles with finite non-zero curvature.

3 Draping smooth obstacles

3.1 Local solutions

We first consider an obstacle that is smooth enough to be represented locally by

$$-z=\left(\frac{\cos^2\psi}{R_1}+\frac{\sin^2\psi}{R_2}\right)\frac{x^2}{2}+\sin\psi\cos\psi\left(\frac{1}{R_1}-\frac{1}{R_2}\right)xy+\left(\frac{\sin^2\psi}{R_1}+\frac{\cos^2\psi}{R_2}\right)\frac{y^2}{2} \\ +\text{cubic terms in } x,\, y, \tag{21}$$

where R_i are the principal radii of curvature at the origin and ψ is the angle between the principal axes of the obstacle and the directions in which the fibres are initially laid down. Thus, the local boundary conditions are $x=0$, $y=v$ on $u=0$ and $x=u$, $y=0$ on $v=0$.

When x and y are expanded in powers of u and v, we find, after some work, that the shear angle γ satisfies

$$8\cos\gamma\sim\sin 2\psi\left[\frac{1}{R_1^2}-\frac{1}{R_2^2}+\left(\frac{1}{R_1}-\frac{1}{R_2}\right)^2\cos 2\psi\right]u^2+\frac{8uv}{R_1R_2} \\ +\sin 2\psi\left[\frac{1}{R_1^2}-\frac{1}{R_2^2}-\left(\frac{1}{R_1}-\frac{1}{R_2}\right)^2\cos 2\psi\right]v^2. \tag{22}$$

This implies that, on a circle $x^2+y^2=\text{constant}$, γ decreases most rapidly in a direction which makes an angle

$$\phi=\frac{1}{2}\arctan\left(\frac{8R_1R_2}{(R_1-R_2)^2\sin(4\psi)}\right) \tag{23}$$

with the x-axis. We note that (23) gives an angle of $\pi/4$ for an axisymmetric surface ($R_1=R_2$) or whenever the fibres are laid down along the principal axes ($\psi=0$ or $\pi/2$).

The calculations become easier in such symmetric configurations, in which case x and y turn out to be sums of powers of u and v respectively, as we will see in the next section. We note that the fibres may be sheared initially so that $x = u + v\cos\gamma_0$ and $y = v\sin\gamma_0$ before being draped, but this does not affect the qualitative response.

3.2 Paraboloids

When the obstacle is a paraboloid of revolution given by $z = (x^2 + y^2)/2$, then (1) becomes

$$x_u^2 + y_u^2 + (xx_u + yy_u)^2 = x_v^2 + y_v^2 + (xx_v + yy_v)^2 = 1. \tag{24}$$

In the special case where $x = x(u)$ and $y = y(v)$, we see that

$$\left(1 + x^2\right)\left(\frac{\mathrm{d}x}{\mathrm{d}u}\right)^2 = \left(1 + y^2\right)\left(\frac{\mathrm{d}y}{\mathrm{d}v}\right)^2 = 1, \tag{25}$$

which can be integrated (subject to $x(0) = y(0) = 0$) to give $x = f(u)$ and $y = f(v)$, where f satisfies the implicit equation

$$f(t)\sqrt{1 + f(t)^2} + \sinh^{-1} f(t) \equiv 2t. \tag{26}$$

The corresponding draped net is shown in Figure 3(a). Note that the solution can be continued further, but we only show the draping of a finite square sheet.

The shear angle is given by

$$\cos\gamma = \frac{xy}{\sqrt{(1 + x^2)\,(1 + y^2)}}. \tag{27}$$

and is $\pi/2$ on $x = 0$ and on $y = 0$, so this solution is indeed generated by the two initial fibres being laid perpendicularly at the vertex of the paraboloid. The shear angle tends to 0 or π as $(x, y) \to \infty$ (other than on the coordinate axes), and again it decreases most rapidly in a direction bisecting the two initial fibres.

We note that an analogous ansatz, with x a function only of u and y a function only of v, works for any smooth surface of the separable form $z = F(x) + G(y)$. For example, a simple extension of the above solution for an axisymmetric paraboloid is for the hyperbolic paraboloid $z = (x^2 - y^2)/2$, which can also be draped with $x = f(u)$ and $y = f(v)$, where f satisfies (26). The net is shown in Figure 3(b) and the contours of the shear angle are exactly the same as those for the paraboloid of revolution.

All these solutions give non-zero values for γ everywhere but this is not always possible with seamless draping as we will now see.

3.3 Tori

The difficulty of seamless draping on simply-connected obstacles is compounded when obstacles have holes. Hence we next consider toroidal obstacles parametrised by

$$\boldsymbol{r}(\theta, \phi) = \begin{pmatrix} (a + b\sin\theta)\cos\phi \\ (a + b\sin\theta)\sin\phi \\ b\cos\theta \end{pmatrix}, \tag{28}$$

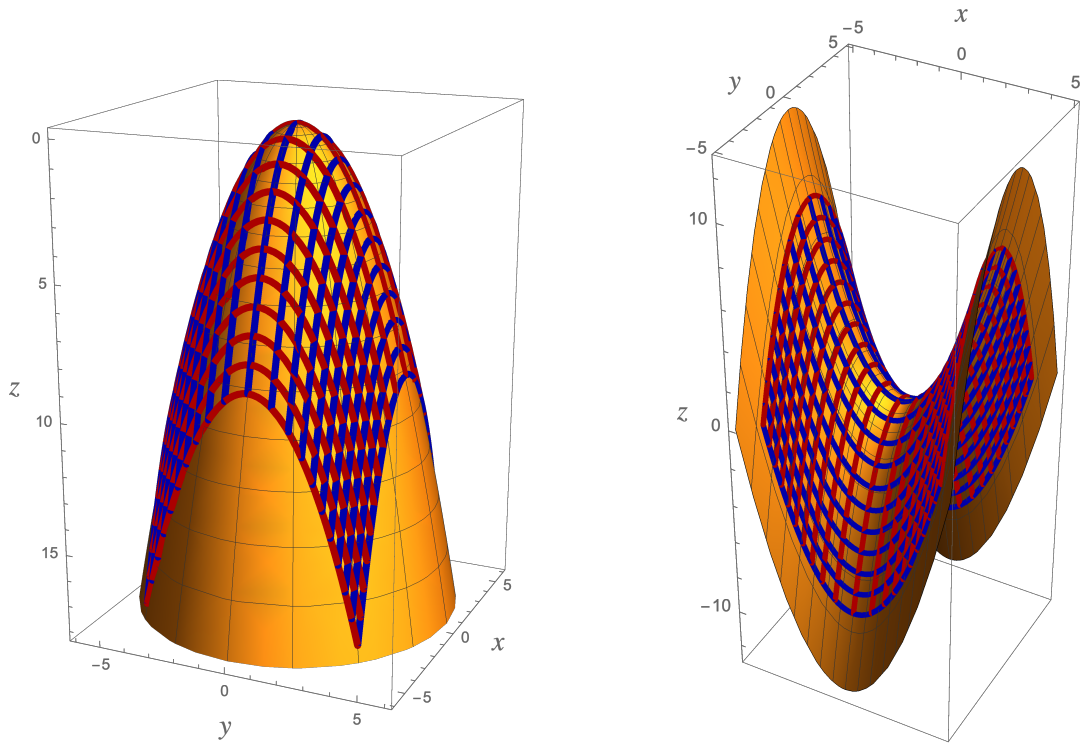

(a) (b)

Figure 3: Draped nets on (a) a paraboloid of revolution, (b) a hyperbolic paraboloid.

with $a > b > 0$, so that (1) gives

$$b^2\theta_u^2 + (a + b\sin\theta)^2\phi_u^2 = b^2\theta_v^2 + (a + b\sin\theta)^2\phi_v^2 = 1. \tag{29}$$

As shown in [9], (29) admit separable solutions, in which

$$\theta = \theta(\xi), \qquad \phi = \phi(\eta), \qquad \xi = u + v, \qquad \eta = u - v. \tag{30}$$

This ansatz is consistent with (29) only if $\phi'(\eta)$ is constant, so, without loss of generality, we set $\phi(\eta) = c\eta$, where c is a positive constant.

The problem (29) then reduces to

$$b^2\left(\frac{\mathrm{d}\theta}{\mathrm{d}\xi}\right)^2 = 1 - c^2(a + b\sin\theta)^2, \tag{31}$$

the general solution of which can be expressed in implicit form involving elliptic functions, which we will not reproduce here. The shear angle is then determined from

$$\sin\left(\frac{\gamma}{2}\right) = c(a + b\sin\theta). \tag{32}$$

Now suppose we begin draping at the top of the torus, so that $\theta(0) = 0$, which is consistent with (31) only if we assume that $c < 1/a$. Then, without loss of generality, we

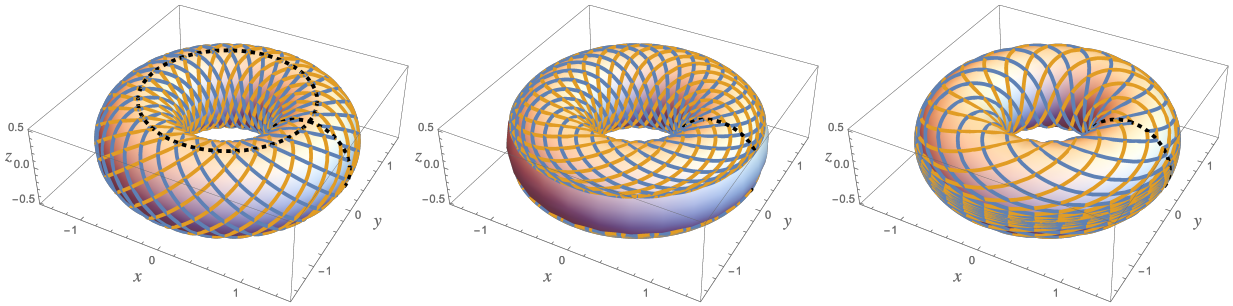

(a) (b) (c)

Figure 4: Three different solutions for a Chebyshev net on a torus with radii $a = 1$, $b = 0.5$ and separation parameter (a) $c = 0.5$, (b) $c = 0.8$, (c) $c = 2/3$.

can take θ to be an increasing function of ξ and we see from (32) that γ can never reach zero. However, it can become equal to π if

$$c(a + b\sin\theta) = 1. \tag{33}$$

We deduce that, with suitable seams, it is possible to cover the entire torus without the shear angle reaching π provided $c < 1/(a+b)$. For intermediate values $1/(a+b) < c < 1/a$, we can start constructing a net from $\theta = 0$, but the solution inevitably terminates with $\gamma = 0$ before the entire torus has been covered.

Figure 4 shows three solutions for a torus with $a = 1$ and $b = 0.5$. In Figure 4(a), we take $c = 0.5 < 1/(a + b)$, so the solution exists on the entire domain θ, $\phi \in [0, 2\pi)$, with seams depicted by black dotted curves at θ, $\phi \in \{0, 2\pi\}$. In Figure 4(b), we take $c = 0.8$. Since $c < 1/a$, we can then integrate (31) in a neighbourhood of $\theta = 0$ but, because $c > 1/(a + b)$, the solution terminates with $\gamma = \pi$ at

$$\theta = \sin^{-1}\left(\frac{1 - ac}{bc}\right), \qquad \text{and} \qquad \theta = -\pi - \sin^{-1}\left(\frac{1 - ac}{bc}\right). \tag{34}$$

Finally, Figure 4(c), shows the borderline case where $c = 1/(a+b) = 2/3$. Now the solution fails precisely when the two sides are about to join together at $\theta = \pi/2$ and $-3\pi/2$.

In the limit where $b \ll a$, the torus approaches a cylinder, which is developable and so can trivially be covered by a "rolling up" a plane net. As the value of b/a increases, the axial curvature of the torus becomes increasingly important, and one might expect that it eventually becomes impossible to cover the entire torus without the shear angle vanishing. The solutions derived here demonstrate that this expectation would be false: regardless of the values of a and b, by choosing c appropriately, one can always find a valid solution on the whole torus. This result is consistent with the constraint (6) because the Euler characteristic of the torus is zero.

3.4 Separable solution for an axisymmetric obstacle

The strategy adopted above for the torus in principle works on any axisymmetric obstacle. We can seek solutions of (9) in separable form with

$$r = r(\xi), \qquad \theta = \theta(\eta), \qquad \xi = u + v, \qquad \eta = u - v. \tag{35}$$

As in §3.3, we find that $\theta'(\eta)$ is constant, and we can set $\theta = c\eta$. Then (9) reduce to

$$\frac{\mathrm{d}r}{\mathrm{d}\xi} = \pm\sqrt{\frac{1 - c^2 r^2}{1 + Z'(r)^2}}, \tag{36}$$

which gives a family of draping solutions, parametrised by c. The shear angle satisfies

$$\cos\gamma = 1 - 2c^2 r^2 \tag{37}$$

and is necessarily zero on the symmetry axis. Thus, this family of solutions cannot describe draping that starts at the axis of, for example, a paraboloid or a sphere. We therefore move on to present a numerical scheme that allows us to compute the solution on any smooth axisymmetric obstacle.

3.5 Numerical solution for an axisymmetric obstacle

We consider an axisymmetric obstacle with a smooth umbilic point at $r = z = 0$ on the surface $z = Z(r)$, so that $Z(r) \sim \kappa r^2/2 + \cdots$ as $r \to 0$. We define new spatial coordinates (ξ, η), given by

$$\xi = A(r)\cos\theta, \qquad \eta = A(r)\sin\theta, \tag{38}$$

where $A(r)$ is chosen to be

$$A = r\exp\left[\int_0^r \frac{\sqrt{1 + Z'(s)^2} - 1}{s}\,\mathrm{d}s\right]. \tag{39}$$

Thus the governing equations (9) are then transformed to

$$\xi_u^2 + \eta_u^2 = \xi_v^2 + \eta_v^2 = F(A), \tag{40}$$

where F is defined parametrically by

$$F(A) = \exp\left[2\int_0^r \frac{\sqrt{1 + Z'(s)^2} - 1}{s}\,\mathrm{d}s\right], \tag{41}$$

along with (39).

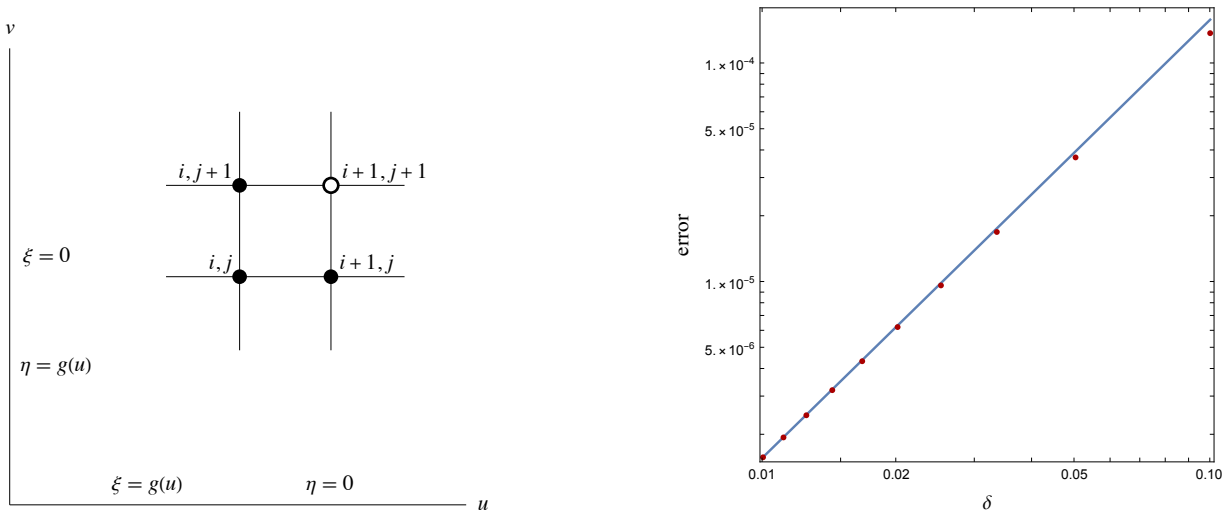

(a) (b)

Figure 5: (a) A schematic showing the boundary conditions and the stencil used for the numerical scheme. (b) The error in the numerical calculation of $x(5,5)$ for a paraboloid plotted versus the grid size δ. The solid line shows the fit error $\sim 0.016\,\delta^2$.

Assuming that two initial fibres are laid perpendicularly at the pole, we may restrict our attention to the quadrant $u, v > 0$, subject to the boundary conditions

$$\xi = g(u),\ \eta = 0 \quad \text{at } u > 0,\ v = 0, \qquad \xi = 0,\ \eta = g(u) \quad \text{at } u = 0,\ v > 0, \tag{42}$$

where g is defined by

$$g\left(\int_0^r \sqrt{1 + Z'(s)^2}\,\mathrm{d}s\right) = r \exp\left[\int_0^r \frac{\sqrt{1 + Z'(s)^2} - 1}{s}\,\mathrm{d}s\right]. \tag{43}$$

Now we discretize the problem on a finite square bounded by the characteristics $u = 0, L$ and $v = 0, L$ for some $L > 0$, using a uniform grid of size $\delta = L/N$, where $N \in \mathbb{N}$. The partial differential equations (40) are approximated up to order δ^2 by the discrete equations

$$\frac{(\xi_{i+1,j} - \xi_{i,j})\,(\xi_{i+1,j+1} - \xi_{i,j+1})}{\delta^2} + \frac{(\eta_{i+1,j} - \eta_{i,j})\,(\eta_{i+1,j+1} - \eta_{i,j+1})}{\delta^2} = \frac{F_{i,j+1} + F_{i+1,j}}{2}, \tag{44a}$$

$$\frac{(\xi_{i,j+1} - \xi_{i,j})\,(\xi_{i+1,j+1} - \xi_{i+1,j})}{\delta^2} + \frac{(\eta_{i,j+1} - \eta_{i,j})\,(\eta_{i+1,j+1} - \eta_{i+1,j})}{\delta^2} = \frac{F_{i,j+1} + F_{i+1,j}}{2}, \tag{44b}$$

where $\xi_{i,j}$ and $\eta_{i,j}$ are the approximations of $\xi(u,v)$ and $\eta(u,v)$ at $(u,v) = (\delta i, \delta j)$, and

$$F_{i,j} = F\left(\sqrt{\xi_{i,j}^2 + \eta_{i,j}^2}\right). \tag{45}$$

Knowing the values of ξ and η at (i,j), $(i+1,j)$ and $(i,j+1)$, the values $\xi_{i+1,j+1}$ and $\eta_{i+1,j+1}$ at the fourth point of the square are given by (44), and the values at $i = 0$ and

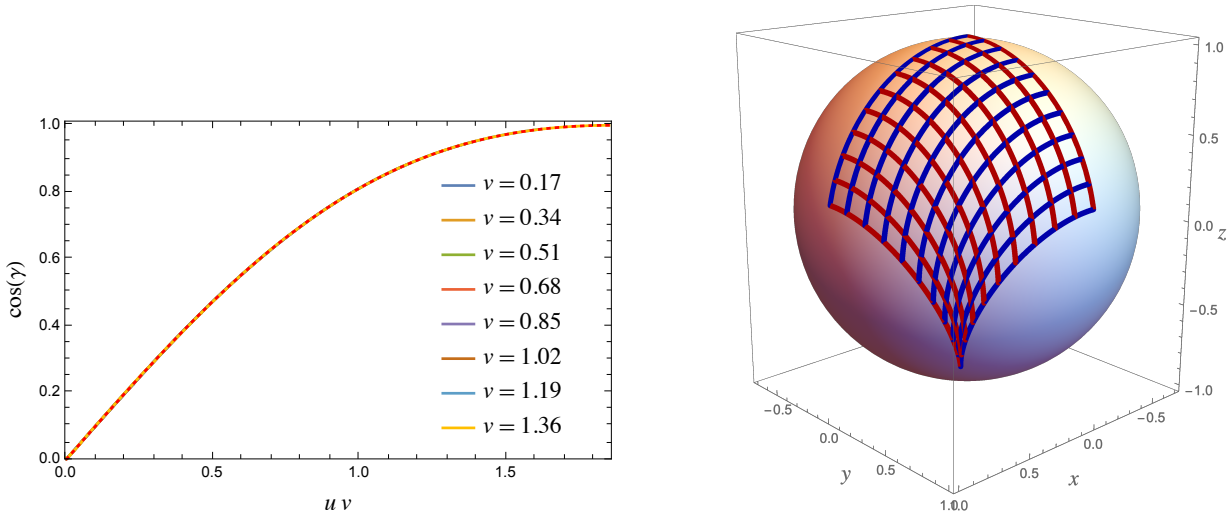

(a) (b)

Figure 6: (a) The cosine of the shear angle γ plotted versus uv for various fixed values of v; the dotted curve shows the similarity solution $\Gamma(uv)$ satisfying (49). (b) Numerical solution for a Chebyshev net on a sphere.

$j = 0$ come from (42). The boundary conditions and the stencil used for the numerical scheme are shown schematically in Figure 5(a).

We first test the proposed scheme on the paraboloid, shown in Figure 3(a) in which $Z(r) = r^2/2$, so that

$$F\left(\frac{2re^{-1+\sqrt{1+r^2}}}{1+\sqrt{1+r^2}}\right) = \frac{4e^{-2+2\sqrt{1+r^2}}}{\left(1+\sqrt{1+r^2}\right)^2}, \tag{46a}$$

$$g\left(\frac{r\sqrt{1+r^2}+\sinh^{-1} r}{2}\right) = \frac{2re^{-1+\sqrt{1+r^2}}}{1+\sqrt{1+r^2}}. \tag{46b}$$

The numerical solution gives the approximation to x at $(u, v) = (5, 5)$ as

$$x(5,5) \approx \frac{\xi_{k,k}}{\sqrt{F_{k,k}}} \quad \text{where} \quad k\delta = 5. \tag{47}$$

However, we know from §3.2 that $x(5,5) = f(5) \approx 2.78682$, where f is given by (26). Figure 5(b) shows that the error between the numerical and analytic solutions decreases quadratically with the grid size δ.

Next we use the same scheme for a spherical obstacle for which the functions F and g are given by

$$F(A) = \left(1+\frac{A^2}{4}\right)^2, \qquad g(u) = 2\tan\left(\frac{u}{2}\right). \tag{48}$$

In this case, analytical solutions for (x, y) are not available but, since the Gaussian curvature K is unity on the sphere, the Sine–Gordon equation (4) admits similarity solutions in which $\gamma = \Gamma(uv)$, where Γ satisfies

$$s\Gamma''(s) + \Gamma'(s) + \sin\Gamma(s) = 0. \tag{49a}$$

For consistency with the boundary conditions in Figure 5(a) we impose $\Gamma(0) = \pi/2$, and the unique solution of (49a) then has asymptotic behaviour

$$\Gamma(s) = \frac{\pi}{2} - s + \frac{s^3}{18} - \frac{7s^5}{1800} + \cdots \quad \text{as } s \to 0; \tag{49b}$$

see [6].

We can compute the shear angle from our numerical solution using

$$\xi_u\xi_v + \eta_u\eta_v = F\left(\sqrt{\xi^2 + \eta^2}\right)\cos\gamma. \tag{50}$$

In Figure 6(a) we show the resulting numerical solution for $\cos\gamma$ (using $\delta = 0.000341$) as a function of uv by varying u while holding v constant. The curves for different values of v all collapse, as expected, confirming that the solution for γ is self-similar although this is not true for ξ and η. Moreover, the numerically computed solution is indistinguishable from the similarity solution $\cos\Gamma(uv)$ obtained from (49). From a practical viewpoint, the key result is that the shear angle γ reaches zero when $uv = u_c^2$, where $u_c \approx 1.3644$.

In Figure 6(b), we show just one quadrant of the net, which could be continued periodically to cover the rest of the upper portion of the sphere. The solution is terminated on the fibres $u = u_c$ and $v = u_c$, which meet at a cusp where γ first reaches zero. The upper limit of the region covered by the net corresponds to the point where $v = 0$ and $u = u_c$ (or *vice versa*), and at this point the height above the equator is given by $z = \cos u_c \approx 0.205$. The lowest point occurs when $(u, v) = (u_c, v_c)$, and we compute the corresponding height as $z \approx -0.6847$, so the net cannot reach the south pole before γ reaches zero. Confirmation comes by integrating along the line $v = u$ and exploiting symmetry to show that γ first reaches zero when

$$z = \cos\left[2\int_0^{u_c} \cos\left(\frac{\Gamma\left(u^2\right)}{2}\right)\,\mathrm{d}u\right], \tag{51}$$

which gives a value of z that differs from our full numerical solution by less than 2×10^{-6}.

By applying the Gauss-Bonnet Theorem (5) with Gaussian curvature $K \equiv 1$, we deduce that the quadrilateral draped region in Figure 6(b) has area equal to $\pi/2$, and therefore covers precisely one half of the surface of the spherical obstacle.

What happens beyond the limiting characteristics shown in Figure 6(b) will be discussed in the next section,

3.6 Draping with small shear angle

We conclude this section by analysing the local fibre geometry near points where γ vanishes.

Without loss of generality, let us fix the coordinates such that the two fibre directions coincide at the origin, where they are parallel to the x-axis. The parametrisation $\boldsymbol{r}(u,v)$ must therefore satisfy

$$\boldsymbol{r}(0,0)=\mathbf{0}, \qquad\qquad \boldsymbol{r}_u(0,0)=\boldsymbol{r}_v(0,0)=(1,0,0)^{\mathrm{T}}. \tag{52}$$

and we assume that, in a neighbourhood of the origin, the obstacle may be approximated by a quadric of the form

$$z\sim\frac{1}{2}\,ax^2+bxy+\frac{1}{2}\,cy^2+\cdots\,, \tag{53}$$

where the local Gaussian curvature is given by $K=ac-b^2$.

Given (52), equations (1) imply that the solution near the origin takes the form

$$x(u,v)\sim(u+v)-\frac{1}{6}\left(a^2(u+v)^3+k_1^2u^3+k_2^2v^3\right)+\cdots\,, \tag{54a}$$

$$y(u,v)\sim\frac{1}{2}\,k_1u^2+\frac{1}{2}\,k_2v^2+\cdots\,, \tag{54b}$$

for some constants k_1 and k_2 which can only be determined globally. The shear angle is then found from

$$\cos\gamma=\boldsymbol{r}_u\cdot\boldsymbol{r}_v\sim1-\frac{1}{2}(k_1u-k_2v)^2+\cdots\,, \tag{55}$$

and hence $\gamma\sim\pm(k_1u-k_2v)$ as $(u,v)\to(0,0)$. We note that γ is generically zero on a line given locally by $k_1u\sim k_2v$, which, in the (x,y)-plane corresponds to

$$y\sim\left(\frac{k_1k_2}{2(k_1+k_2)}\right)x^2. \tag{56}$$

This curve is locally a parabola which is tangent to the fibre direction at the origin; it does not involve the local Gaussian curvature and therefore the behaviour does not depend on whether the surface is developable or not.

Figure 7 shows an example where we take $a=c=-1$ and $b=0$ so the surface is locally a paraboloid of revolution, for plotting convenience shifted by -0.1 in the z-direction. The other parameters are set to $k_1=-0.5$ and $k_2=1$. Figure 7(a) shows the resulting net draped over the surface, for values of u and v between -0.5 and 0; the projection of the solution onto the (x,y)-plane is also shown. The fibre directions become parallel, at $x=y=0$, $u=v=0$. In Figure 7(b), the darker curves reproduce the projection onto the (x,y)-plane from Figure 7(a), and now we can also show the lighter curves that reveal the behaviour with the ranges of u and v extended to the region $-1<u<-2v<1$. In this case, the shear angle is zero when $u+2v=0$, whose image in the (x,y)-plane is indicated by the dotted curve; as predicted, this curve is locally parabolic and tangent to the cusp at the origin.

In the example shown in Figure 7, the curvatures k_1 and k_2 of the fibre directions meeting at the cusp are chosen to differ, so that the structure is asymmetric. In cases where the geometry imposes reflectional symmetry, for example the spherical net shown in

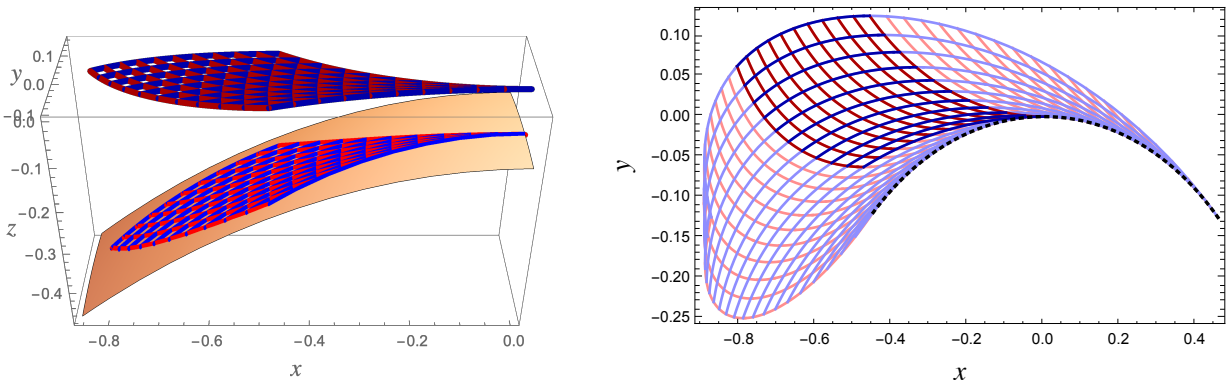

(a) (b)

Figure 7: (a) Local behaviour of a net on a paraboloid $z = -0.1 - 0.5\,(x^2 + y^2)$ near a zero of the shear angle γ; also shown is the projection onto the (x, y)-plane. (b) The continuation of the solution from (a).

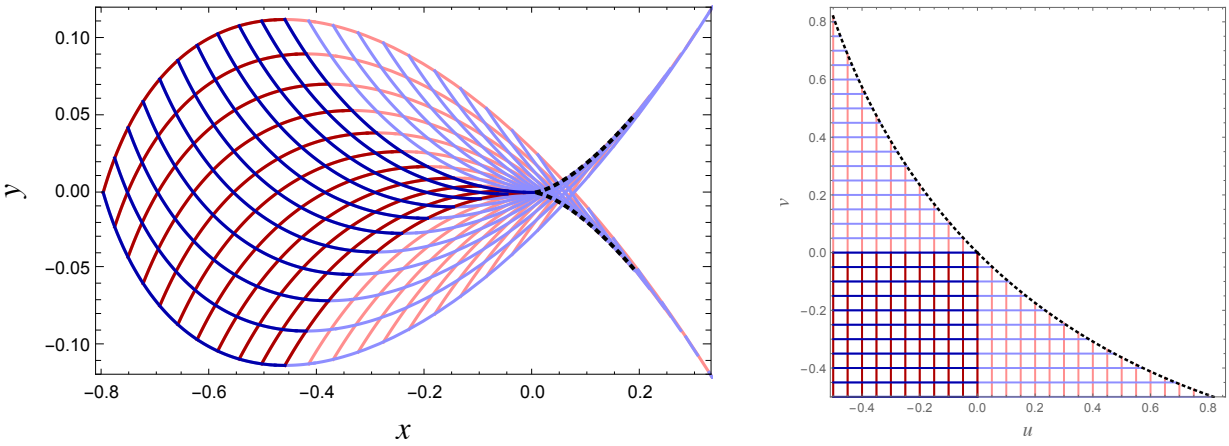

(a) (b)

Figure 8: (a) The projection onto the (x, y)-plane of a symmetric net near a zero of the shear angle γ, with parameter values $a = 1$, $k_1 = 0.8025$, $k_3 = 0.09803$. The dotted curve shows the local behaviour (59) of the cusp. (b) The pre-image of (a) in the (u, v)-plane.

Figure 6(b), the fibre curvatures satisfy $k_1 + k_2 = 0$, and the curve on which $\gamma = 0$ becomes degenerate, according to (56). In such cases, we need to proceed to higher order to obtain the form of the local envelope.

Let us therefore consider a surface given locally by (53) with $b = 0$, so it has the required symmetry about the x-axis. The corresponding expansions for x and y take the forms

$$x(u,v) \sim (u+v) - \frac{1}{6}\left[a^2(u+v)^3 + k_1^2\left(u^3+v^3\right)\right] + \frac{3k_1k_3}{4}\left(u^4+v^4\right) + \cdots \tag{57a}$$

$$y(u,v) \sim \frac{k_1}{2}\left(u^2-v^2\right) + k_3\left(v^3-u^3\right) + \cdots, \tag{57b}$$

where k_1 and k_3 are globally-determined constants and

$$\gamma(u,v) \sim -k_1(u+v) + 3k_3\left(u^2+v^2\right) + \cdots. \tag{58}$$

It follows that γ vanishes on a curve whose image in the (x,y)-plane is given by

$$\begin{pmatrix} x \\ y \end{pmatrix} \sim 2k_1k_3 \begin{pmatrix} 3s^2 \\ 2k_1^2 s^3 \end{pmatrix} \quad \text{as } s \to 0, \tag{59}$$

and we therefore expect to see the fibre directions becoming parallel on a curve with a 2/3-power cusp, rather than the locally parabolic curve seen in Figure 7(b).

We can apply this theory to the spherical example in Figure 6(b) where we know that $\gamma(u,v) = \Gamma(uv)$, and Γ satisfies (49). Expanding about the singularity at $(u,v) = (u_c, v_c)$, we get

$$\gamma\left(u_c+\tilde{u}, u_c+\tilde{v}\right) \sim u_c\Gamma'\left(u_c^2\right)\left(\tilde{u}+\tilde{v}\right) + \Gamma'\left(u_c^2\right)\tilde{u}\tilde{v} + \frac{1}{2}u_c^2\Gamma''\left(u_c^2\right)\left(\tilde{u}+\tilde{v}\right)^2 + \cdots, \tag{60}$$

and, from (49), we have $u_c^2\Gamma''\left(u_c^2\right) = -\Gamma'\left(u_c^2\right)$. Therefore (60) is indeed of the same form as (58), and we can read off the values

$$k_1 = -u_c\Gamma'\left(u_c^2\right) \approx 0.8025, \qquad k_3 = -\frac{1}{6}\Gamma'\left(u_c^2\right) \approx 0.09803. \tag{61}$$

Figure 8(a) shows the local pattern of characteristics given by (57) with the parameters given by (61) and $a = 1$. The darker curves show the image in the (x,y)-plane of the square $(u,v) \in [-0.5, 0] \times [-0.5, 0]$, which is equivalent to that seen on the sphere in Figure 6(b). The lighter curves again show the results of extending the ranges of (u,v) to positive values of u and v. We terminate each characteristic when the fibre angle reaches zero: we can see that this occurs on the dotted cusped curve given locally by (59). However, here the fibres begin to cross over each other before reaching the branch of the cusp at which they become parallel, giving an indication of the singular behaviour to be expected when attempting to extend the sphere draping solution from Figure 6(b) beyond the first zero of the shear angle γ.

Figure 8(b) shows the pre-image of Figure 8(a) in the (u, v)-plane. Again, the dotted curve shows where the fibre angle γ reaches zero and where the fibres have been terminated. If one were to trim the fabric along this curve, we anticipate that the behaviour illustrated in Figure 8(a) would lead to the existence of two overlapping sheets of fabric in the region between the two dotted curves. If such a geometric configuration occurred in the characteristics of a hyperbolic system of conservation laws, it would lead to a shock wave which could be modelled by a weak solution. Here, the possibility of overlapping layers means that multi-valuedness need not be unphysical.

The results of this section have demonstrated that continuous draping of a smooth non-developable obstacle is often not possible without seams or creases since the non-zero Gaussian curvature can induce distortions of the net that result in the shear angle reaching zero before the entire obstacle can be covered. In the next section we extend our analysis to describe piecewise smooth obstacles that contain edges and/or vertices.

4 Draping non-smooth obstacles

4.1 Local solutions

We first focus attention on the local draping behaviour near an edge in an otherwise smooth obstacle. The resulting disruption to the fibre geometry depends on whether or not one of the fibres lies along the edge; if it does then, following the discussion in §2, it is possible for γ to have a jump discontinuity across the edge. Indeed, it is in principle possible to shear the material even on a smooth surface such that γ has a discontinuity across a fibre.

Consider a general surface which is everywhere continuous, but whose normal is discontinuous across a curve Γ, say. As usual, we seek a parametrisation $\boldsymbol{r} = \boldsymbol{r}(u, v)$ of the surface satisfying (1), with the shear angle determined by (2). We parametrise Γ by $\boldsymbol{r} = \boldsymbol{r}_e(s) = \boldsymbol{r}\big(u_e(s), v_e(s)\big)$, where $(u, v) = \big(u_e(s), v_e(s)\big)$ represents Γ in the (u, v)-plane; the tangent to Γ is

$$\boldsymbol{t} = \boldsymbol{r}_e'(s) = u_e'(s)\boldsymbol{r}_u\big(u_e(s), v_e(s)\big) + v_e'(s)\boldsymbol{r}_v\big(u_e(s), v_e(s)\big). \tag{62}$$

Both $\boldsymbol{r}$ and $\boldsymbol{t}$ are continuous on Γ, and the continuity of $|\boldsymbol{t}|^2$, gives the condition

$$u_e'v_e'\big[\cos\gamma\big]_-^+ = 0, \tag{63}$$

where $\big[\cdot\big]_-^+$ denotes the jump in a quantity across the edge. It follows from (63) that the shear angle γ is continuous across the edge, unless either $u_e' = 0$ or $v_e' = 0$, in other words unless the edge is tangent to a characteristic.

By taking the scalar product of (62) with $\boldsymbol{r}_u$ and $\boldsymbol{r}_v$ and using (63), we obtain the further jump conditions

$$u_e'\big[\boldsymbol{t}\cdot\boldsymbol{r}_u\big]_-^+ = v_e'\big[\boldsymbol{t}\cdot\boldsymbol{r}_v\big]_-^+ = 0. \tag{64}$$

The implication is that the angle between the edge and the fibre direction $\boldsymbol{r}_u$ must be continuous unless the edge is parallel to $\boldsymbol{r}_v$, and *vice versa*. Thus, the components of the

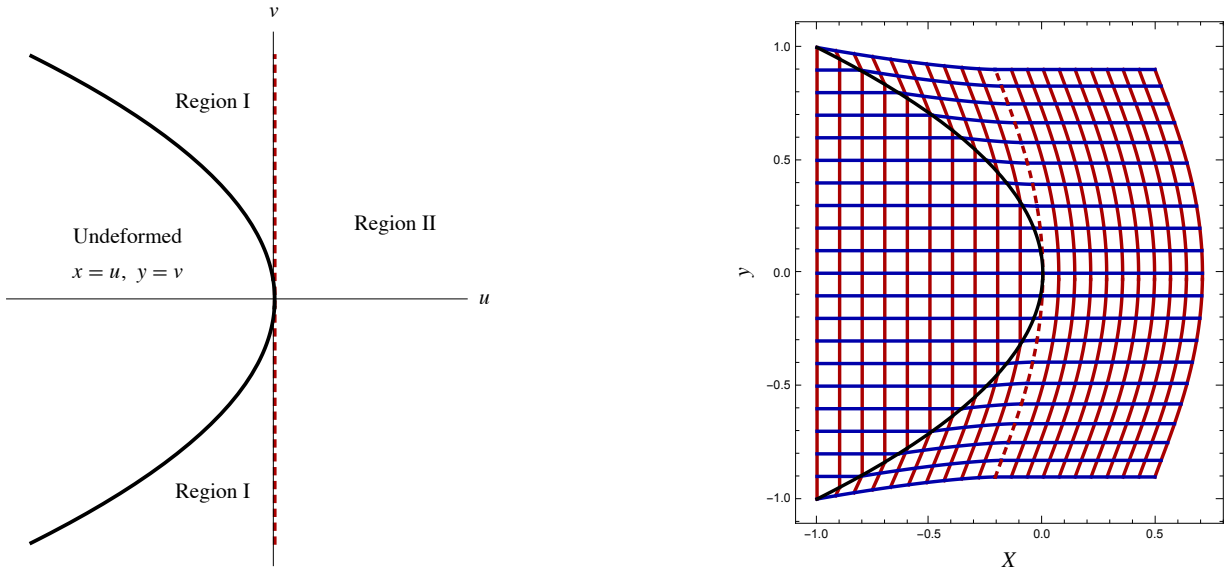

(a) (b)

Figure 9: (a) Schematic of the (u, v)-plane showing the edge $u = -\epsilon v^2$ in the obstacle (black curve) and the characteristic $u = 0$ that is tangent to the edge (red dashed line). (b) The projection of the characteristics given by (67) and (69) on the (X, y)-plane, here with $\epsilon = 0.5$ and $\theta = \pi/4$. Again, the black curve shows the edge $X = -y^2$ and the dashed curve shows the characteristic $U = 0$.

fibre direction vectors parallel to the surface do not change as they cross the edge, except where the edge is tangent to a characteristic.

To illustrate what happens at such points, we look at the case where undeformed material lies on a flat table $z = 0$ for $x < -\epsilon y^2$, and then drapes over the nearly planar quadric

$$z = -\tan\theta\left(x + \epsilon y^2\right) \quad \text{for } x > -\epsilon y^2, \tag{65}$$

where $0 < \epsilon \ll 1$. In the limit $\epsilon \to 0$, the obstacle is simply two planes intersecting along the y-axis at an angle $\pi - \theta$. The fibres on the table are given by $x = u$ and $y = v$ so that the edge $x = -\epsilon y^2$ is tangent to the fibre $u = 0$ at the origin as seen in Figure 9(a).

We need to consider separately the solution in the regions indicated in Figure 9(a). There is an undistorted region in $u < -\epsilon v^2$, a region I between the edge and the characteristic fibre $u = 0$ and the region II in which $u > 0$. We can exploit the smallness of ϵ by noting that u and x are both small in region I when $v = O(1)$. In terms of the normalised variables $U = u/\epsilon$ and $X = x/\epsilon$, the governing equations (1) in region I are transformed to

$$\epsilon^{-2} y_U^2 + X_U^2 + \tan^2\theta (X_U + 2y y_U)^2 = y_v^2 + \epsilon^2 X_v^2 + \epsilon^2 \tan^2\theta (X_v + 2y y_v)^2 = 1, \tag{66a}$$

subject to the continuity conditions

$$X = U, \; y = v \quad \text{on} \quad U = -v^2. \tag{66b}$$

When $\epsilon \ll 1$, the asymptotic solution to the problem (66) is given by

$$X(U,v) \sim U\cos\theta - v^2(1-\cos\theta) + \cdots , \tag{67a}$$

$$y(U,v) \sim v + \frac{4\epsilon^2}{3}(1-\cos\theta)\left((-U)^{3/2}\,\mathrm{sign}(v) - v^3\right) + \cdots . \tag{67b}$$

The shear angle in region I is then found from

$$\begin{aligned}\cos\gamma &= \epsilon^{-1}y_U y_v + \epsilon X_U X_v + \epsilon\tan^2\theta(X_U + 2yy_U)(X_v + 2yy_v)\\ &\sim 2\epsilon(1-\cos\theta)\left(v - \mathrm{sign}(v)\sqrt{-U}\right) + \cdots .\end{aligned} \tag{68}$$

Thus $\cos\gamma = 0$ at $U = -v^2$ and the shear angle is continuous across the edge up to order ϵ; as shown above, it must in fact be continuous at all orders. The tangency of the edge to the characteristic $U = 0$ does, however, result in a square-root singularity in γ as U approaches zero from below.

To extend the solution into region II, we impose continuity of x and y across the characteristic $U = 0$, but this is not sufficient to specify the solution uniquely: we also need data on the characteristics $U =$ constant that emanate from region II. For definiteness, we continue the fibre $v = 0$ into region II, by imposing $y(U,0) = 0$ for $U > 0$. Then for $\epsilon \ll 1$ the asymptotic solution in region II is

$$X(U,v) \sim U\cos\theta - v^2(1-\cos\theta) + \cdots , \tag{69a}$$

$$y(U,v) \sim v - \frac{4\epsilon^2}{3}(1-\cos\theta)v^3 + \cdots , \tag{69b}$$

and

$$\cos\gamma \sim 2\epsilon(1-\cos\theta)v + \cdots . \tag{70}$$

Thus γ is continuous also across $U = 0$, albeit with the square-root singularity as the characteristic is approached from the left-hand side.

In Figure 9(b) we plot the asymptotic solution derived above in the (X,y)-plane with $\theta = \pi/4$ and a large value of $\epsilon = 0.5$ so that the distortion of the fibres is clearly visible. Although γ is continuous, one can detect a singularity in the fibre curvature as the characteristic $U = 0$ (indicated by the dashed curve) is approached. We will see that such behaviour is typical on a characteristic that grazes an edge in an otherwise smooth surface.

A similar analysis can be performed when the obstacle is given by $z = 0$ for $x < \epsilon y^2$ and $z = -\tan\theta\,(x - \epsilon y^2)$ for $x > \epsilon y^2$. We again have to solve separately in the two regions III and IV, as shown in Figure 10(a), but the altered geometry introduces the additional complication that the edge $x = \epsilon y^2$ in the (u,v)-plane is now unknown in advance; this curve is denoted by $u = F(v)$ as shown in Figure 10(a). In addition, the solution in region III depends on information from the characteristic $v = 0$ (indicated by a blue dashed curve), while the solution in region IV depends on information from the characteristic $u = 0$ (indicated by a red dashed curve). Therefore the problems in regions III and IV are coupled and must be solved simultaneously.

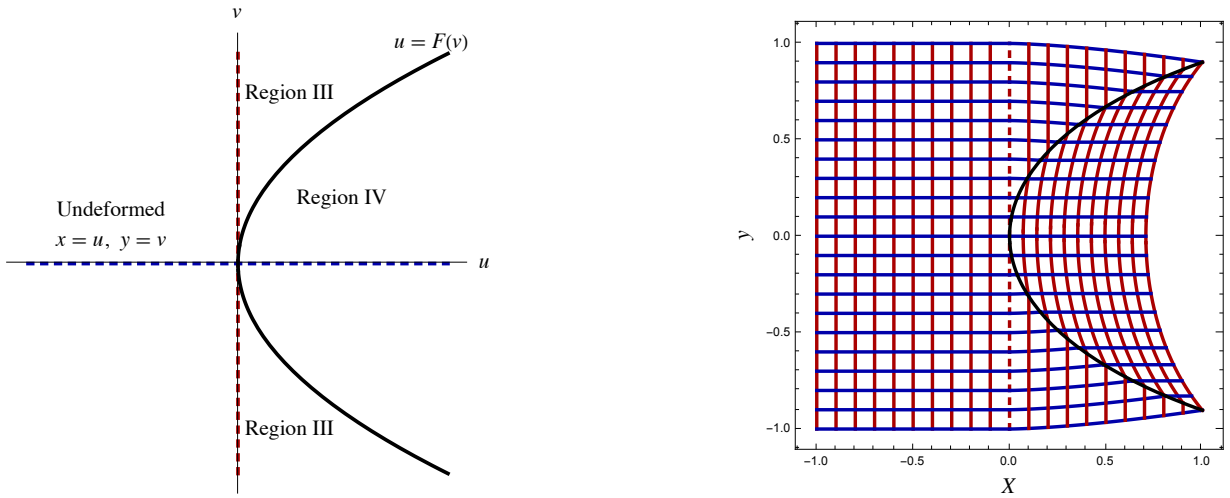

(a) (b)

Figure 10: (a) Schematic of the (u, v)-plane showing the curve $u = F(v)$ corresponding to the edge $x = \epsilon y^2$ in the obstacle (black curve) and the characteristics $u = 0$ and $v = 0$ that are tangent and perpendicular to the edge (red and blue dashed line). (b) The projection of the asymptotic solution given by (71) and (72) on the (X, y)-plane, here with $\epsilon = 0.5$ and $\theta = \pi/4$. Again, the black curve shows the edge $X = y^2$ and the dashed curve shows the characteristic $U = 0$.

In terms of the rescaled variables $X = x/\epsilon$ and $U = u/\epsilon$, the solutions for X and y may again be expressed as asymptotic expansions in powers of ϵ^2. In region III,

$$X(U, v) \sim U + \cdots , \tag{71a}$$

$$y(U, v) \sim v - \frac{4\epsilon^2}{3}(1 - \cos\theta)U^{3/2}\,\mathrm{sign}(v) + \cdots , \tag{71b}$$

$$\gamma \sim \frac{\pi}{2} + 2\epsilon(1 - \cos\theta)\,\mathrm{sign}(v)\sqrt{U} + \cdots , \tag{71c}$$

and in region IV,

$$X(U, v) \sim U\cos\theta + v^2(1 - \cos\theta)\cdots , \tag{72a}$$

$$y(U, v) \sim v - \frac{4\epsilon^2}{3}(1 - \cos\theta)v^3 + \cdots , \tag{72b}$$

$$\gamma \sim \frac{\pi}{2} + 2\epsilon(1 - \cos\theta)v + \cdots . \tag{72c}$$

The boundary between the two regions in the (U, v)-plane is given by

$$U \sim v^2 - \frac{\epsilon^2}{3}(1 - \cos\theta)(5 + 3\cos\theta)v^4 + \cdots \tag{73}$$

and the projection onto the (X, y)-plane of the asymptotic solution is shown in Figure 10(b), again taking $\theta = \pi/4$ and $\epsilon = 0.5$. We observe that the shear angle γ is still continuous

everywhere, and again has a square root singularity as the grazing characteristic $U = 0$ is approached from region III.

We next consider the global behaviour of draping solutions on surfaces with edges, as well as the more extreme singularity that occurs when the obstacle has a vertex.

4.2 Draping a piecewise developable surface

In practice, there is often interest in draping obstacles that comprise two or more developable surfaces joined together along edges. Each developable section may be unwrapped onto a plane, upon which a general drape may be constructed as in §2. However, we must now ensure that the resulting drapes connect smoothly across the joins between the developable surfaces so that seamless draping can be achieved.

We suppose that two developable surfaces, joined at an edge, have been separated and flattened out onto the (x, y)-plane. The edge between the two surfaces is flattened onto two planar boundaries, which are denoted by $\boldsymbol{r} = \boldsymbol{r}_0^+(s)$ and $\boldsymbol{r}_0^-(s)$, where s is arc-length. We denote the corresponding tangents by

$$\frac{\mathrm{d}\boldsymbol{r}_0^\pm}{\mathrm{d}s} = \begin{pmatrix} \cos\theta^\pm \\ \sin\theta^\pm \end{pmatrix}. \tag{74}$$

The general solution for the drape on the planar surface on either side of the join is given as in (20) by

$$\boldsymbol{r}(u, v) = \boldsymbol{f}^\pm(u) + \boldsymbol{g}^\pm(v), \tag{75}$$

where $\boldsymbol{f}^\pm$ and $\boldsymbol{g}^\pm$ have derivatives denoted by

$$\frac{\mathrm{d}\boldsymbol{f}^\pm}{\mathrm{d}u} = \begin{pmatrix} \cos\alpha^\pm \\ \sin\alpha^\pm \end{pmatrix}, \qquad \frac{\mathrm{d}\boldsymbol{g}^\pm}{\mathrm{d}v} = \begin{pmatrix} \cos\beta^\pm \\ \sin\beta^\pm \end{pmatrix}. \tag{76}$$

As shown in §4.1, to ensure that draping is possible, the angle between each fibre direction and the edge must be continuous when the boundaries are joined together, so we impose the jump conditions

$$\alpha^+ - \alpha^- = \beta^+ - \beta^- = \theta^+ - \theta^-, \tag{77}$$

which are equivalent to requiring u and v to be continuous across the edge. Thus, if $(u, v) = \big(u_0(s), v_0(s)\big)$ on the edge, then

$$\boldsymbol{r}_0^\pm(s) = \boldsymbol{f}^\pm\big(u_0(s)\big) + \boldsymbol{g}^\pm\big(v_0(s)\big). \tag{78a}$$

Now suppose that we prescribe the functions $\boldsymbol{f}^-(u)$ and $\boldsymbol{g}^-(v)$ and are given the locations $\boldsymbol{r}_0^\pm$ of the two branches of the edge. We can then in principle use (78a) to solve first for u_0 and v_0 and then for $\boldsymbol{f}^+$ and $\boldsymbol{g}^+$.

In the simplest configuration, we suppose that the fibres are laid straight and perpendicular on the "$-$" side of the edge, with

$$\boldsymbol{f}^-(u) = \begin{pmatrix} u \\ 0 \end{pmatrix}, \qquad \alpha^-(u) = 0, \qquad \boldsymbol{g}^-(v) = \begin{pmatrix} 0 \\ v \end{pmatrix}, \qquad \beta^-(u) = \frac{\pi}{2}. \tag{79}$$

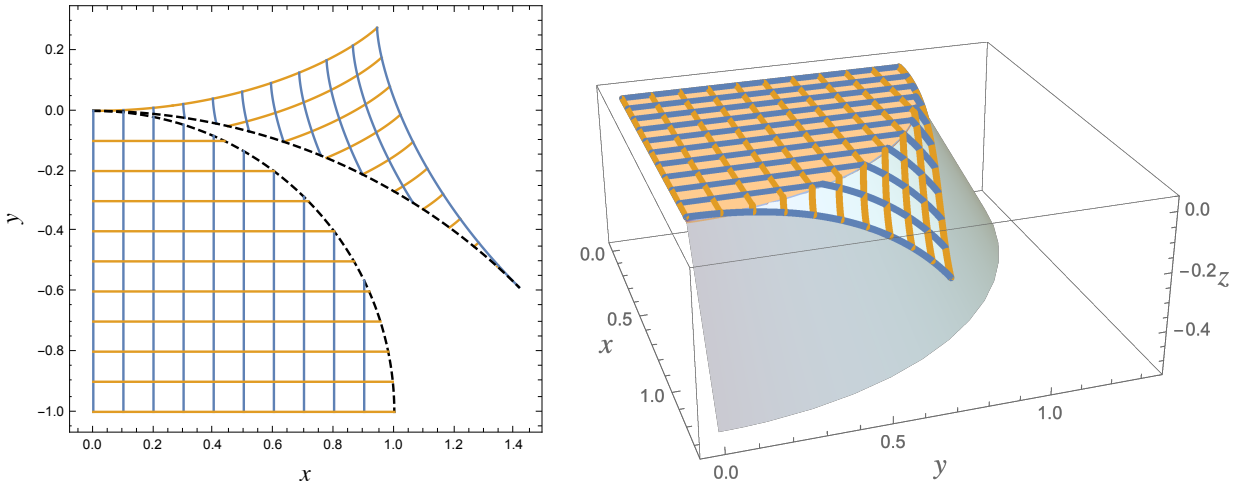

(a) (b)

Figure 11: (a) The join between two flattened developable surfaces whose boundaries are circular arcs. (b) The three-dimensional shape obtained when the boundaries are connected, corresponding to draping a net over a truncated cone. The characteristics $u =$ constant and $v =$ constant are shown as blue and orange curves, respectively.

From (78a), we find u_0 and v_0 using

$$\boldsymbol{r}_0^-(s) = \begin{pmatrix} x_0^-(s) \\ y_0^-(s) \end{pmatrix} = \begin{pmatrix} u_0(s) \\ v_0(s) \end{pmatrix}, \tag{80}$$

and thence

$$\boldsymbol{r}_0^+(s) = \begin{pmatrix} x_0^+(s) \\ y_0^+(s) \end{pmatrix} = \boldsymbol{f}^+\big(x_0^-(s)\big) + \boldsymbol{g}^+\big(y_0^-(s)\big). \tag{81}$$

By differentiating with respect to s and rearranging, we find

$$\frac{\mathrm{d}}{\mathrm{d}s}\left(\boldsymbol{f}^+(x_0^-(s))\right) = \cos\theta^- \begin{pmatrix} \cos\left(\theta^+ - \theta^-\right) \\ \sin\left(\theta^+ - \theta^-\right) \end{pmatrix} = \frac{1}{2}\begin{pmatrix} \cos\left(\theta^+\right) + \cos\left(2\theta^- - \theta^+\right) \\ \sin\left(\theta^+\right) - \sin\left(2\theta^- - \theta^+\right) \end{pmatrix}, \tag{82a}$$

$$\frac{\mathrm{d}}{\mathrm{d}s}\left(\boldsymbol{g}^+(y_0^-(s))\right) = \sin\theta^- \begin{pmatrix} -\sin\left(\theta^+ - \theta^-\right) \\ \cos\left(\theta^+ - \theta^-\right) \end{pmatrix} = \frac{1}{2}\begin{pmatrix} -\cos\left(\theta^+\right) + \cos\left(2\theta^- - \theta^+\right) \\ \sin\left(\theta^+\right) + \sin\left(2\theta^- - \theta^+\right) \end{pmatrix}. \tag{82b}$$

To determine $\boldsymbol{f}^+(u)$ and $\boldsymbol{g}^+(v)$, we just have to integrate with respect to s and then invert the functions $x_0^-(s)$ and $y_0^-(s)$. This final step is possible provided x_0^- and y_0^- are strictly monotonic functions.

4.3 Draping circular edges

We now adapt the above procedure to describe draping the frustum of a circular cone. This situation is shown in Figure 11(a), where the two flattened boundaries are circular

arcs. We scale to make the radius of the smaller circle equal to 1, so we have

$$\theta^-(s) = -s, \qquad \theta^+(s) = -\kappa^+ s, \tag{83}$$

with $0 \le \kappa^+ < 1$. Integration of (82) produces

$$\boldsymbol{f}^+\left(x_0^-(s)\right) = \frac{1}{2}\begin{pmatrix} \dfrac{\sin\left((2-\kappa^+)s\right)}{2-\kappa^+} + \dfrac{\sin\left(\kappa^+ s\right)}{\kappa^+} \\ \dfrac{1-\cos\left((2-\kappa^+)s\right)}{2-\kappa^+} - \dfrac{1-\cos\left(\kappa^+ s\right)}{\kappa^+} \end{pmatrix}, \tag{84a}$$

$$\boldsymbol{g}^+\left(y_0^-(s)\right) = \frac{1}{2}\begin{pmatrix} \dfrac{\sin\left(\kappa^+ s\right)}{\kappa^+} - \dfrac{\sin\left((2-\kappa^+)s\right)}{2-\kappa^+} \\ -\dfrac{1-\cos\left((2-\kappa^+)s\right)}{2-\kappa^+} - \dfrac{1-\cos\left(\kappa^+ s\right)}{\kappa^+} \end{pmatrix}. \tag{84b}$$

We then invert

$$x^-(s) = \sin s = u, \qquad y^-(s) = -1 + \cos s = v \tag{85}$$

to give $\boldsymbol{f}^+$ and $\boldsymbol{g}^+$ as

$$\boldsymbol{f}^+(u) = \frac{1}{2}\begin{pmatrix} \dfrac{\sin\left((2-\kappa^+)\sin^{-1}(u)\right)}{2-\kappa^+} + \dfrac{\sin\left(\kappa^+\sin^{-1}(u)\right)}{\kappa^+} \\ \dfrac{1-\cos\left((2-\kappa^+)\sin^{-1}(u)\right)}{2-\kappa^+} - \dfrac{1-\cos\left(\kappa^+\sin^{-1}(u)\right)}{\kappa^+} \end{pmatrix} \qquad (0 \le u \le 1), \tag{86a}$$

$$\boldsymbol{g}^+(v) = \frac{1}{2}\begin{pmatrix} \dfrac{\sin\left(\kappa^+\cos^{-1}(v+1)\right)}{\kappa^+} - \dfrac{\sin\left((2-\kappa^+)\cos^{-1}(v+1)\right)}{2-\kappa^+} \\ \dfrac{1-\cos\left((\kappa^+-2)\cos^{-1}(v+1)\right)}{\kappa^+-2} + \dfrac{\cos\left(\kappa^+\cos^{-1}(v+1)\right)-1}{\kappa^+} \end{pmatrix} \qquad (-1 \le v \le 0). \tag{86b}$$

The solution on the "+" side of the edge is then given by $\boldsymbol{r}(u,v) = \boldsymbol{f}^+(u) + \boldsymbol{g}^+(v)$ for $u^2+(v+1)^2 > 1$. We note that an analogous solution was obtained in [18,19] by considering a truncated pyramid in the limit as the number of faces tends to infinity. The upper section of Figure 11(a) shows the resulting net produced when we take $\kappa^+ = 1/2$. When the two boundaries (marked by black dashed curves) are joined, with the quarter-circular region held flat, the upper section is mapped onto a frustum, as shown in Figure 11(b). which illustrates the result of draping a square net over a "lampshade".

In Figure 11, we see that the characteristics are tangent to the boundary at the end points of the circular boundaries, and the characteristics through these end points delineate a finite distorted triangular domain in which the upper solution is fully determined by the

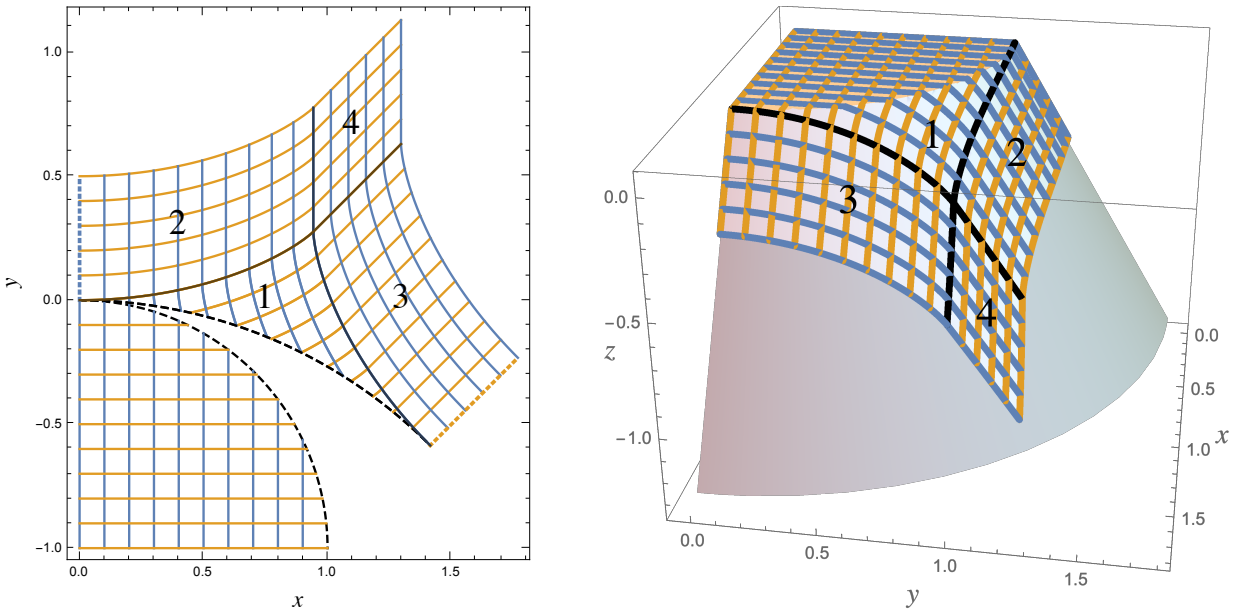

(a) (b)

Figure 12: The net from Figure 11 extended beyond the edge of the circle $x^2 + y^2 = 1$.

jump conditions across the edge. To continue the solution further, we proceed as in §4.1 to pin the fibres $u = 0$ and $v = 0$ along generators of the cone. This enables us to extend the characteristics through the end points on straight lines perpendicular to the edge, as indicated by the blue and orange dotted lines, respectively, in Figure 12(a). This choice means that the unflattened net covers one quarter of the "lampshade" shaped obstacle, as shown in Figure 12(b), and may be extended by symmetry to cover the entire obstacle. This is the global continuation of the local solution presented in §4.1.

Analytically, the resulting solution shown in Figure 12 is obtained by extending the definitions (86) of $\boldsymbol{f}^+$ and $\boldsymbol{g}^+$ to

$$\boldsymbol{f}^+(u) = \frac{1-\kappa^+}{\kappa^+(2-\kappa^+)}\begin{pmatrix}0\\-1\end{pmatrix} + \left[u + \frac{(1-\kappa^+)^2}{\kappa^+(2-\kappa^+)}\right]\begin{pmatrix}\sin(\pi\kappa^+/2)\\ \cos(\pi\kappa^+/2)\end{pmatrix} \quad (u>1), \tag{87a}$$

$$\boldsymbol{g}^+(v) = \begin{pmatrix}0\\ v\end{pmatrix} \quad (v>0). \tag{87b}$$

The possible choices of the signs of $(u-1)$ and v divide the solution in the upper section into four regions. In the region marked 1 in Figure 12(a), where $u < 1$ and $v < 0$, the solution is as shown previously in Figure 11(a). In regions 2 and 3, we have $\{u < 1,\, v > 0\}$ and $\{u > 1,\, v < 0\}$, respectively. In either case, one family of characteristics originates at the edge, while the other comes from the perpendicularly extended boundary of the domain. Finally, in region 4, we have $u > 1$ and $v > 0$, so the functions $\boldsymbol{f}^+$ and $\boldsymbol{g}^+$ are both given by equation (87) and the characteristics are all straight lines, with both α^+ and

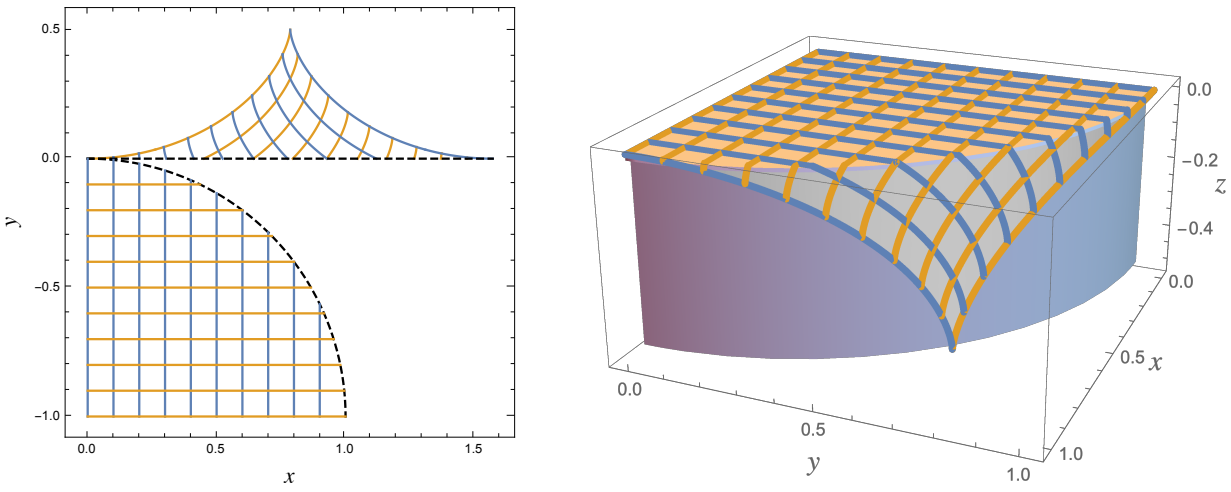

(a) (b)

Figure 13: (a) The join between a circular arc of unit radius and a flat edge, (b) The sheet draped over a cylinder formed by joining the two edges.

β^+ constant and given respectively by

$$\alpha^+ = \frac{\pi}{2}\left(1 - \kappa^+\right), \qquad \beta^+ = \frac{\pi}{2}. \tag{88}$$

The minimum value of the shear angle γ is attained in region 4, and thus given by

$$\gamma_{\min} = \frac{\pi\kappa^+}{2}. \tag{89}$$

The shear angle reaches zero in the limiting case where $\kappa^+ = 0$, which corresponds to joining a straight edge to a disc to form a circular cylindrical obstacle, as shown in Figure 13.

Figure 13(a) shows the characteristic picture in the flattened (x, y)-plane when $\kappa^+ = 0$ and the upper edge is a straight line. The shear angle approaches zero at the top corner of the upper section, where the two edge characteristics meet. Figure 13(b) shows the three-dimensional picture formed when the two edges are joined, corresponding to draping a sheet over a truncated circular cylinder. This figure illustrates that some wrinkling will is unavoidable when a square tablecloth is spread over a circular table.

In the solutions shown in Figures 11–13, we have chosen a uniform orthogonal net on the flat portion of the frustum, with $\alpha_- = 0$ and $\beta_- = \pi/2$. It follows from (77) that the maximum value of α and minimum value of β on the "+" side are given by

$$\max \alpha^+ = \Delta_{\max}, \qquad \min \beta^+ = \frac{\pi}{2} + \Delta_{\min}, \tag{90}$$

respectively, where $\Delta_{\max}$ and $\Delta_{\min}$ are the maximum and minimum values of $\theta^+ - \theta^-$ on the join. It follows that γ reaches zero on the "+" side if and only if

$$\Delta_{\max} - \Delta_{\min} \geq \frac{\pi}{2}. \tag{91}$$

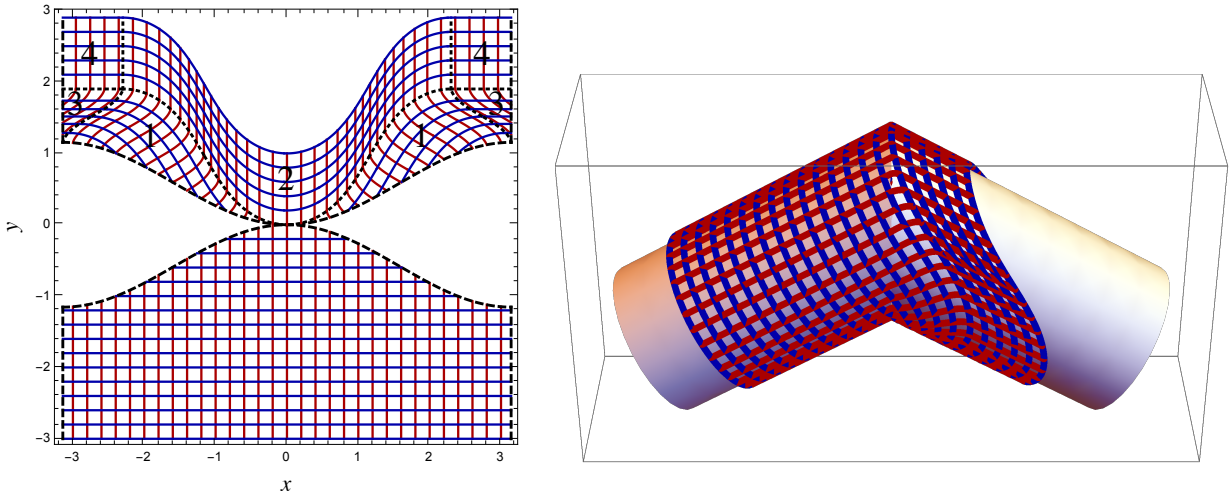

(a) (b)

Figure 14: (a) The projected net on two flattened-out joined cylinders, (b) The three–dimensional drape formed when the two edges are joined ($m = \pi/3$).

Figure 13 shows a marginal case where γ has only just reached zero, and indeed we have $\Delta_{\max} = \pi/2$ and $\Delta_{\min} = 0$ in agreement with (91). Indeed, γ will reach zero in a finite distance whenever the difference in inclination angle between the top and bottom branches of the edge varies varies by at least $\pi/2$.

4.4 Draping intersecting Cylinders

We now consider draping a pair of identical circular cylinders joined at an angle of $2m$ when one cylinder is draped with the fibres along and perpendicular to its generators. There will inevitably be a seam along the bottom generator but we now show how the "knee" can be draped smoothly. When the two cylinders are cut apart along the join and then flattened out, the net is as shown in Figure 14(a), where x and y correspond to azimuthal and axial distance, respectively, along the surfaces of the two cylinders. We have taken the radii of the cylinders equal to unity, so x varies between $-\pi$ and π. The two branches of the join are given by $y = \pm \cot m\big(1 - \cos x\big)$ or, parametrically in terms of arc-length s,

$$\begin{pmatrix} x_0^{\pm}(s) \\ y_0^{\pm}(s) \end{pmatrix} = \begin{pmatrix} f_2(s) \\ \pm \cot m\big(1 - \cos f_2(s)\big) \end{pmatrix}, \tag{92}$$

where f_2 satisfies

$$\frac{\mathrm{d}f_2}{\mathrm{d}s} = \frac{1}{\sqrt{1 + \cot^2 m \sin^2 f_2}}, \qquad f_2(0) = 0. \tag{93}$$

With the inclination angles α and β defined as in §4.2, on the left-hand cylinder we have $\alpha^-(s) \equiv 0$ and $\beta^-(s) \equiv \pi/2$. The solution on the right-hand side of the edge is then

found by integrating (82). Since

$$\theta^+ = -\theta^- = \tan^{-1}(\cot m \sin f_2), \tag{94}$$

(82) may be integrated, using (93), and then inverted to give

$$\boldsymbol{f}^+(u) = \begin{pmatrix} -u + 2\sin m \tan^{-1}(\csc m \tan u) \\ -\sin m \log\left(\frac{(1-\cos m)(1+\cos m \cos u)}{(1+\cos m)(1-\cos m \cos u)}\right) \end{pmatrix}, \tag{95a}$$

$$\boldsymbol{g}^+(v) = \begin{pmatrix} 2\cos^{-1}(1+v\tan m) - 2\sin m \tan^{-1}\left(\frac{\csc m\sqrt{-v\tan m(2+v\tan m)}}{1+v\tan m}\right) \\ -v + \sin m \log\left(\frac{(1-\cos m)(1+v\sin m+\cos m)}{(1+\cos(m))(1-v\sin m-\cos m)}\right). \end{pmatrix} \tag{95b}$$

The solution on the right-hand section produced by imposing continuity across the join is then given by $\boldsymbol{r}(u,v) = \boldsymbol{f}^+(u) + \boldsymbol{g}^+(v)$.

The expressions (95) hold on the domain $-\pi < u < \pi$ and $-\cot m(1-\cos u) < v < 0$, corresponding to the values of (u,v) on the characteristics intersecting the edge from $v < 0$. The bounding characteristics on which $v = 0$, $u = \pi$ or $u = -\pi$ are indicated by dotted black curves in Figure 14(a), where we can see that they enclose a region, labelled "1", in which the solution is determined by (95). To extend the solution further, we have to impose more boundary conditions on the upper section ($v > 0$).

First, we extend to positive values of v by assuming symmetry about the line $x = 0$, so that $\beta^+ = \pi/2$ when $u = 0$. This choice corresponds to replacing (95b) by

$$\boldsymbol{g}^+(v) = \begin{pmatrix} 0 \\ v \end{pmatrix} \quad \text{for } v > 0, \tag{96}$$

and extends the solution into the region labelled "2" in Figure 14(a).

Next we consider values of $u > \pi$ and $u < -\pi$ to extend the net to cover the whole cylinder $-\pi < x < \pi$. As in the case of the lampshade, the simplest choice is to take $\alpha^+ = 0$ to ensure that the characteristics $v =$ constant intersect $x = \pm\pi$ normally. Then, imposing continuity with (95a) at $x = \pi$, we find

$$\boldsymbol{f}^+(u) = \begin{pmatrix} u \\ 0 \end{pmatrix} + \begin{pmatrix} -2\pi(1-\sin m) \\ 4\sin m \log\big(\cot(m/2)\big) \end{pmatrix} \quad \text{for } u > \pi, \tag{97}$$

with an analogous expression for $u < -\pi$. We thus extend the solution into the regions labelled "3" in Figure 14(a).

Finally, when $v > 0$ and $|u| > \pi$, the choices (96) and (97) imply that we again have an orthogonal net, with $\alpha^+ = 0$ and $\beta^+ = \pi/2$, as shown in the regions labelled "4" in Figure 14(a). Figure 14(b) shows the final result of rolling the solution from Figure 14(a) onto the two joined cylinders, and demonstrates that we can successfully drape a sheet over the joined cylinders without the shear angle γ reaching zero. In general, one can show

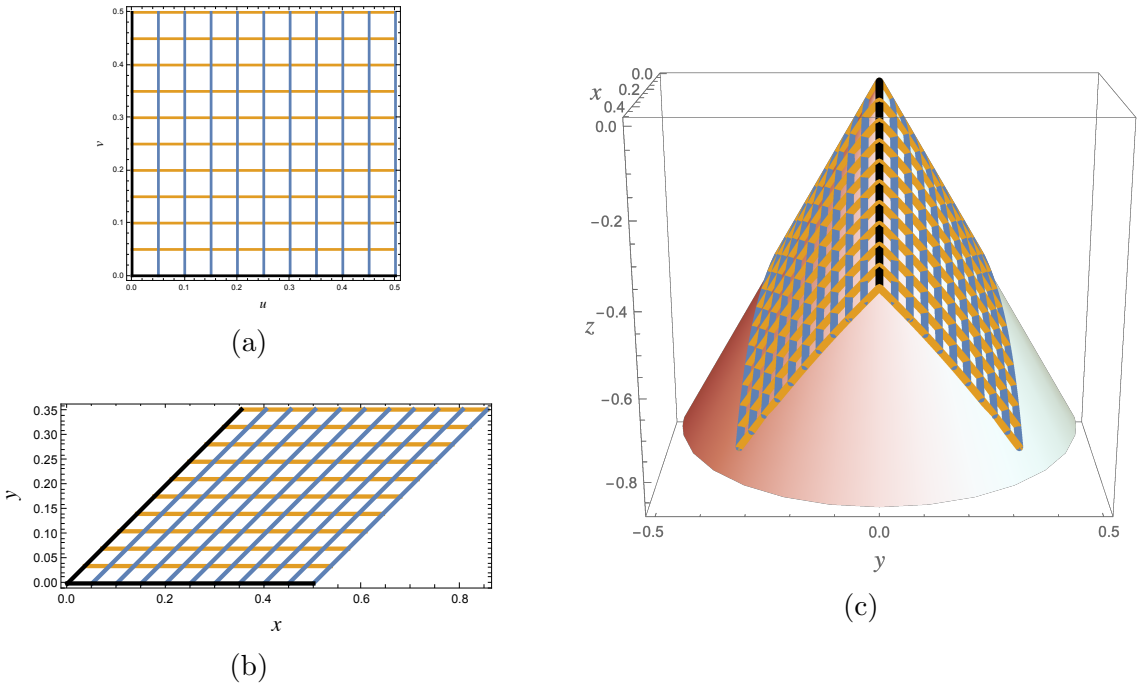

(a)

(b)

(c)

Figure 15: (a) Undeformed material in the quadrant $u, v > 0$. (b) The same material sheared through an angle $\pi \sin\theta/2$. (c) The resulting draping of a cone with apex angle θ (here equal to $\pi/6$).

that the construction outlined above works for any angle $2m$ such that $m > \pi/4$, and that the minimum shear angle is given by

$$\gamma_{\min} = 2\left(m - \frac{\pi}{4}\right). \tag{98}$$

However the minimum shear angle reaches zero whenever $m \leq \pi/4$, implying that it is not possible to cover the entire structure when the cylinders meet orthogonally or at an acute angle.

4.5 Draping cones and corners

In order to drape the tip of a cone we will show that it is necessary to create discontinuities in the shear angle in the material. We suppose that the fibres $u = 0$ and $v = 0$ are placed over the tip of a right circular of angle θ and lie along the generators of the cone in perpendicular planes. Thus, as illustrated in Figure 15, the angle between the two fibres on the cone surface must be reduced from $\pi/2$ in the undeformed state to $\pi \sin\theta/2$ when draped over one quarter of the cone surface. The material in each quadrant of the (u, v)-plane therefore has to be sheared to an angle $\gamma = \pi \sin\theta/2$ and there will inevitably be discontinuities in the shear angle (and also in $\boldsymbol{r}_u$, $\boldsymbol{r}_v$) across the characteristics $u = 0$ and $v = 0$. Note that if the top of the lampshade in Figure 12(a) is reduced in area, the region 4

of uniform shear takes up more of the area of the cone. This process may be continued until the solution shown in Figure 15 is reached when the area of the top vanishes and the lampshade becomes a cone.

A similar approach can be used for any cone or pyramid. If for instance we wish to drape a corner made up of three planes intersecting at right angles, then the fibres that spanned an angle 2π in the plane need now to span three right angles. Thus if each quadrant of the u, v plane is sheared equally, the angle of shear in each quadrant must be reduced from $\pi/2$ to $3\pi/8$. This will allow the corner to be draped smoothly but it will not be possible to arrange the material symmetrically on the three faces. This method to drape polygonal obstacles has been described in [18, 19].

5 Conclusions

In this paper, we have shown how the continuum limit of a Chebyshev net provides a model that can shed light on difficulties that may be encountered in draping a woven sheet over a curved obstacle. The resulting mathematical insights largely depend on the fact that the two families of fibres in the draped sheet can be identified with the characteristics of the nonlinear system (1) of partial differential equations governing the configuration of the net on the obstacle. Thus the fibres carry information across the sheet and may propagate configurational discontinuities. Also, mathematical singularities occur when members of the two families of fibres become tangential to each other, and this gives an indication of likely local creasing in practice. By performing a local analysis, we have categorised the generic behaviour to be expected in the vicinity of such a singularity.

We have shown that fundamental results from differential geometry allow one to make some quite general statements about the possibility of smoothly draping different classes of obstacles. We have also shown that, despite the nonlinearity, one can find several families of explicit solutions for a range of obstacles, both smooth and with edges. We then demonstrated a numerical discretisation, based on the fact that fibres are characteristics, which in principle allows solutions to be computed on any smooth obstacle. The creation of seams and/or discontinuities of the shear angle in different regions of the draped material that are bounded by fibres can further enlarge the range of drapable obstacles.

Our idealised model is purely geometrical, and does not describe the mechanical properties of the fibre sheet, and the role of gravity in draping is also completely ignored. In addition, we note that there remain open questions concerning the existence, uniqueness and smoothness of solutions of (1) especially for the Goursat problem in which the draped position of one fibre from each family is prescribed.

6 Acknowledgements

We would like to thank Professor Shankar Venkataramani (University of Arizona) and participants of the European Study Group with Industry 138 for helpful discussions during

the preparation of this paper. We also thank a Reviewer for drawing our attention to some important references.

We are glad to have the opportunity to applaud Graeme Wake's great achievements in promoting applied mathematics around the world, especially in New Zealand and the Pacific Rim. We very much hope that he will continue to inspire young researchers to adopt his insightful and sympathetic style for years to come.

References

[1] C. Baek, A. D. Sageman-Furnas, M. K. Javed & P. M. Reis, 2018, Form finding in elastic gridshells, *Proc. Nat. Acad. Sci.* **115**, 75–80.

[2] D. Barton, H. Ockendon, B. Piette & R. Whittaker, 2018, New techniques for composite wing manufacture, Study Group Report, ESGI138, Bath, `http://www.maths-in-industry.org/miis/754/`.

[3] L. Bianchi, 1922, *Lezioni di Geometria Differenziale* Vol. 1, 3rd ed. 153–162, Spoerri, Pisa.

[4] E. Cerda, L. Mahadevan & J. M. Pasini, 2004, The elements of draping, *Proc. Nat. Acad. Sci.* **101**, 1806–1810.

[5] E. D. Demaine & J. O'Rourke, 2007, *Geometric folding algorithms: linkages, origami, polyhedra*, Cambridge.

[6] É. Ghys, 2011, Sur la coupe des vêtements: Variation autour d'un thème de Tchebychev. *L'Enseignement Mathématique* **57**(1), 165–208.

[7] J. N. Hazzidakis, 1879, Ueber einige Eigenschaften der Flächen mit constantem Krúmmungsmaass, *Journal für die reine und angewandte Mathematik* **88**, 68–73.

[8] C. Jiang, T. Gast & J. Teran, 2017, Anisotropic elastoplasticity for cloth, knit and hair frictional contact, *ACM Trans.Graph.* **36**, 152:1–152:14.

[9] J. Koenderink & A. van Doorn, 1998, Shape from Chebyshev nets, *European Conference on Computer Vision*, 215–225. Springer.

[10] Y. Masson & L. Monasse, 2017, Existence of global Chebyshev nets on surfaces of absolute Gaussian curvature less than 2π, *J. Geom.* **108**, 25–32.

[11] J. Mitani & T. Igarishi, 2011, Interactive design of planar curved folding by reflection, *Pacific Graphics Short Papers.*

[12] J. Ockendon, S. Howison, A. Lacey & A. Movchan, 2003, *Applied Partial Differential Equations*, Oxford.

[13] A. Papadopoulos, 2016, Euler and Chebyshev: From the sphere to the plane and backwards, `arXiv:1608.02724`.

[14] A. C. Pipkin, 1986 Equilibrium of Tchebychev Nets. In: *The Breadth and Depth of Continuum Mechanics*. Springer, Berlin, Heidelberg.

[15] S. Poincloux, M. Adda-Bedin & F. Lechenault, 2018, Geometry and elasticity of a knitted fabric, *Phys. Rev. X* **8**, 021075.

[16] J. R. Postle & R. Postle, 1999, The dynamics of fabric drape, *Textile Res. J.* **69**, 623–629.

[17] G. Quinn & C. Gengnagel, 2014, A review of elastic grid shells, their erection methods and the potential use of pneumatic formwork. In: *Mobile and Rapidly Assembled Structures IV*, ed. N. De Temmerman & C. A. Brebbia (WIT Press, Southampton, UK), 129–145.

[18] R. E. Robertson, T.-J. Chu, R. J. Gerard, J.-H. Kim, M. Park, H.-G. Kim & R. C. Peterson, 2000, Three-dimensional fiber reinforcement shapes obtainable from flat, bidirectional fabrics without wrinkling or cutting. Part 1. A single four-sided pyramid, *Composites Part A: Applied Science and Manufacturing* **31**(7), 703–715.

[19] R. E. Robertson, T.-J. Chu, R. J. Gerard, J.-H. Kim, M. Park, H.-G. Kim & R.C. Peterson, 2000, Three-dimensional fiber reinforcement shapes obtainable from flat, bidirectional fabrics without wrinkling or cutting. Part 2: a single n-sided pyramid, cone, or round box, *Composites Part A: Applied Science and Manufacturing* **31**(11), 1149–1165.

[20] S. L. Samelson & W. P. Dayawansa, 1995, On the existence of global Tchebychev nets *Trans. Amer. Math. Soc.* **347**(2), 651–660.

[21] M. Servant, 1902, Sur l'habillage des surfaces, *C. R. Acad. Sci.* **135**, 575–577.

[22] M. Servant, 1903, Sur l'habillage des surfaces. *C. R. Acad. Sci.* **137**, 112–115.

[23] D. J. Steigmann, 2018, Continuum theory for elastic sheets formed by inextensible crossed elasticae, *Int. J. Non-linear Mech.* **106**, 324–329.

[24] W. B. Wang & A. C. Pipkin, 1985, Inextensible networks with bending stiffness, *Q. J. Mech. Appl. Math.* **39**, 343–359.

[25] C. E. Weatherburn, 1955, *Differential Geometry of three dimensions*, Cambridge.

[26] T. J. Willmore, 1959, *An Introduction to Differential Geometry*, Oxford.